GAS TURBINE COMBUSTION MODELING FOR A PARAMETRIC EMISSIONS MONITORING SYSTEM

by

UELI HONEGGER

B.E. University of Applied Science of Rapperswil, Switzerland, 2004

A THESIS

submitted in partial fulfillment of the requirements for the degree

MASTER OF SCIENCE

Department of Mechanical and Nuclear Engineering
College of Engineering

KANSAS STATE UNIVERSITY
Manhattan, Kansas

2007

Approved by:

Major Professor
Kirby S. Chapman, Ph.D.

Abstract

Oxides of nitrogen (NO_x), carbon monoxide (CO) and other combustion by-products of gas turbines have long been identified as harmful atmospheric pollutants to the environment and humans. Various government agencies place restrictions on emissions and often require some sort of emissions monitoring even for new low emission gas turbines. Predicting actual emissions from operating parameters that affect the formation of pollutants, called parametric emissions monitoring system (PEMS), has potential economic advantages compared to a continuous emissions monitoring system (CEMS). The problem is that a simple applicable PEMS does not exist.

During this study, a gas turbine combustor model applying first engineering principles was developed to predict the emission formation of NO_x and CO in a gas turbine. The model is based on a lean-premixed combustor with a main and pilot burner including the function of a bleeding air valve. The model relies on ambient condition and load. The load is expressed as a percentage of the target speed of the gas producer turbine. Air flow and fuel flow for the main and pilot burner are calculated by the model based on the load through a set of measured input data for a specific gas turbine. To find the combustion temperature characteristics, the combustor is divided into several zones. The temperature for each zone is calculated by applying an energy balance. To predict NO_x and CO, several correlations explored by various researchers are used and compared against each other, using the calculated temperatures, pressures and equivalence ratios.

A comparison between collected emissions examples from a turbine test cell data spreadsheet and predicted emissions by the developed model under the same conditions show a highly accurate match for NO_x emission at any load. Because of the high variation of CO at part load, the model predictions only match the CO data set at full load.

Table of Contents

List of Figures

List of Tables

Acronyms

CDP	Compressor Discharge Pressure
CEMS	Continuous Emissions Monitoring System
CT	Combustion Turbine
DLN	Dry Low NOx
GPT	Gas Producer Turbine
IMSL	International Mathematical and Statistical Library
KSU	Kansas State University
NGML	National Gas Machinery Laboratory
PEMS	Parametric Emissions Monitoring System
PFR	Plug-Flow Reactor
PRCI	Pipeline Research Council International
PSR	Perfectly-Stirred Reactor
PT	Power Turbine
WSR	Well-Stirred Reactor

Nomenclature

A	Area
AF	Air/fuel ratio
c_p	Specific heat (kJ/(kg T))
D_0	Drop diameter
E	Energy
FA	Fuel/air ratio
f_c	Combustion fraction (varies 0-1)
G	Gibbs function
h	Heat-transfer coefficient
HHV	Higher heating value
K_p	Chemical equilibrium constant
L	Luminosity
LHV	Lower heating value
M	Molecular weight
m	Mass
$\dot{m}$	Mass flow rate
N	Mole number
K	Heat transfer conduction
p	Pressure
PR	Pressure ratio
$\dot{Q}$	Heat transfer rate
q	Specific heat transfer
R	Gas specific gas constant, R_u / M
r	Radius
R_u	Universal gas constant (kJ/(kmol K) or (kPa $m^{3)}$/(kmol K))
T	Temperature

t	Time
v	Velocity
V	Volume
$\dot{V}$	Volumetric flow rate
Zr	Fraction reactants
Zp	Fraction products

Greek Variables

Δ	Change in a condition, as in ΔT is the change in temperature
ε	Emissivity
ϕ	Fuel-air based equivalence ratio [FA/FA_{stoich}]
γ	Ratio of the specific heats
η	Efficiency
λ_{eff}	Effective evaporation constant
μ	Dynamic viscosity
ρ	Density
σ	Stefan-Boltzmann constant, 5.67×10^{-8} W/(m^2K^4)

Subscripts

a	Air
act	Actual
ad	Adiabatic process
amb	Ambient conditions
C	Combustion
comp	Compressor
corr	Corrected
e	Evaporation
eff	Effective
ex	Exhaust
f	Fuel
g	Gas
i	Species within a mixture
in	Inlet
out	Discharge or outlet of a system
P	Products
pz	Primary zone
s	Isentropic
sat	Saturation
st	Standard
stoich	Stoichiometric
tot	Total
turb	Turbine
w	Wall

Units

atm	Atmosphere
K	Kelvin
°C	Celsius
ppmv	Parts per million by volume
rpm	Revolution per minute
s	Second
hr	Hour
min	Minute

Chemical Substances

C_2H_6	Ethane
CH_4	Methane
CO	Carbon Monoxide
CO_2	Carbon Dioxide
H, H_2	Hydrogen
HCN	Hydrogen cyanide
H_2O	Water
N, N_2	Nitrogen
NO_x	Nitrogen Oxides
O, O_2	Oxygen
OH	Hydroxyl

Acknowledgements

This thesis is the most significant scientific accomplishment in my life so far. It would never have been possible without the people who supported me and believed in me. I first want to thank my advisor Dr. Kirby S. Chapman, the director of the National Gas Machinery Laboratory (NGML). He gave me the opportunity to work on this research for my master thesis. He always took time for me to discuss my issues even when he was busy. I only can hope my next boss will have the same friendly and encouraging attitude he has. I want to thank Dr. Ali Keshavarz, assistant director at the NGML, for his insightful support and helpful comments. He made clear to me various issues I had about my research. I also want to thank all my colleagues at the NGML who made my office a great place to work. I am grateful for their help and support, especially during the time I suffered from a serious sport injury. I also want to thank Dr. Donald L. Fenton and Dr. Bruce R. Babin to be a member in my defense committee.

This research has been supported and founded by the Pipeline Research Council International (PRCI). I thank them for confidence in the NGML, Dr. Chapman and me. I am also grateful for the Department of Mechanical and Nuclear Engineering at the Kansas State University for providing me an excellent work environment during the past years. I am thankful to SOLAR Turbines Incorporation, especially Dr. Rainer Kurz, for their support and discussion during my research.

An individual thanks goes to my roommates and friends I found during my time as a college student in Manhattan KS. Being thousand of miles away from where I grew up, they gave me the feeling of being at a second home. I hope I will keep in touch with all of them. At the end, I also want to thank my parents and my siblings. They taught me the good things that really matter in life. I am glad and proud to be part of the Honegger family.

Ueli Honegger
July 2007
Manhattan, KS, USA

CHAPTER 1 - Introduction

During the period from the granting of the first patent in 1791 to the present, gas turbines have been developed into very reliable, versatile engines. Figure 1-1 shows a cut of a typical two shaft industrial gas turbine, the type of turbine this research is focused on. The main components are an air compressor, a combustor, a gas generator turbine and a power turbine. The compressor takes in outside air and then compacts and pressurizes the air molecules through a series of rotating and stationary compressor blades. In the combustor, fuel is added to the pressurized air molecules and ignited. The heated molecules expand and move at high velocity into the gas generator turbine section. The turbine converts the energy from the high velocity gas into useful rotational power though expansion of the heated compressed gas over a series of turbine rotor blades.

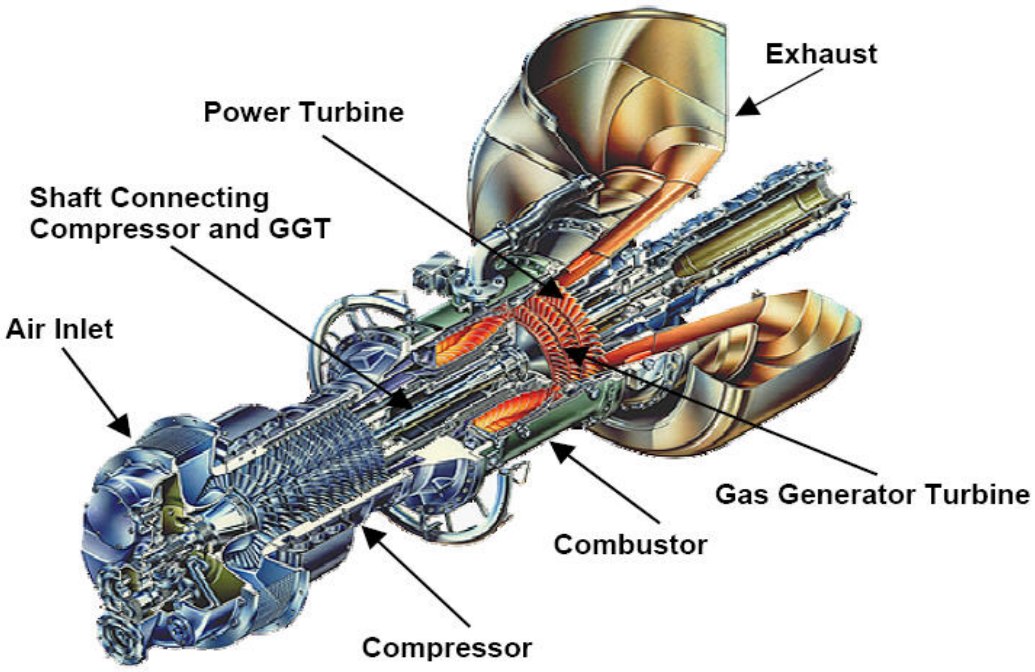

Figure 1-1 Typical two shaft gas turbine

Source: (Kurz, et al. 2003)

After leaving the gas generator turbine, the gas still has a relatively high pressure and temperature. It is now further expanded in the power turbine. The power turbine is connected to the driven equipment like a dynamometer or a pipeline compressor. In a two shaft turbine, the driven equipment will run at a speed that is independent of the speed of the gas generator.

As fuel, industrial gas turbines used in the natural gas transmission industry typically run on natural gas. Natural gas burns cleaner than other fossil fuels, such as oil and coal, and produces less greenhouse gas per unit energy release (Lefebvre. 1999). The primary component of natural gas is methane (CH_4) with about 93 percent, the shortest and lightest hydrocarbon molecule. It also contains a small amount of heavier hydrocarbon gases such as ethane (C_2H_6), propane (C_3H_8) and butane (C_4H_{10}).

Pollutant emissions from combustion processes such as oxides of nitrogen (NO_x) or carbon monoxide (CO) have become of great public concern due to their impact on health and the environment. The past decade has witnessed rapid changes both in the regulations for controlling gas turbine emissions and in the technologies used to meet these regulations. Monitoring the emissions is typically performed with a Continuous Emissions Monitoring System (CEMS). A CEMS monitors emissions by directly sampling the exhaust gas. In addition to the high initial cost of a CEMS (around $150,000 - $170,000), there are significant annual costs for calibration and maintenance (around $30,000 – $35,000) (Jones, et al. 2005). These high costs together with the increased emissions monitoring requirements for industrial gas turbines created a demand for a lower cost emission monitoring system, using easily measured operating parameters, and then correlate these operating parameters to end-stack emissions. Such a system is referred to as a Parametric Emissions Monitoring System (PEMS). A PEMS is less complex, does not require periodic calibration using expensive calibration gases, and can be incorporated into gas turbine systems that are already used to measure most of the appropriate parameters.

Objectives

A review of the literature indicates that globally an applicable PEMS for combustion turbines does not exist. Because of this, a PEMS that is easily usable to a variety of gas turbine engines is desired. In order to build up such a PEMS system, the objectives of this thesis research are:

- Develop a combustor model applying first engineering principles to determine combustion turbine emissions (NO_x and CO) based on a selected set of easily-measured parameters; and
- Demonstrate that the governing relationships are accurate and reliable by comparing the predicted results to a set of measured test data.

The available literature indicates that lean-premixed combustion is the most widely used NO_x reduction design strategy. Because of this, the model is based on a lean premixed combustion system. The basics about the combustion process plus a review of the literature on how the NO_x and CO formation happens is found in the literature review in Chapter 2. Chapter 3 describes the physical relations of the developed combustor model. How the model is built and the techniques used to solve it can be found in Chapter 4. A validation of the provided data from a existing gas turbine is done in Chapter 5. Chapter 6 shows the comparison between the predicted results from the developed model with the measured data. The conclusion of this work and the next steps for continuing the research will be in the last Chapter 7.

CHAPTER 2 - Literature Review

The first part of the literature review explains the basics of the combustion process with carbon hydrogen fuels and gives an overview of the different available combustor types. The second part focuses on the emissions including several studies of CO and NO_x formation processes. This research was necessary to gain an understanding of the physics taking place during the CO and NO_x formation in a gas turbine combustor and also to select an appropriate technique for modeling the process. The last part of the literature review focuses on the current PEMS technology. This was done to provide a comprehensive understanding of what techniques have been employed to develop a PEMS.

Combustion Processes

Combustion is a chemical reaction during which a fuel is oxidized and a large quantity of energy is released (Çengel, et al. 2002). In the literature, it is distinguished between complete combustion and incomplete combustion. It is often instructive to study the combustion of a fuel by assuming that the combustion is complete. However, when dealing with actual combustion processes, they most likely are incomplete.

Complete Combustion Process

A combustion process is complete if all the carbon in the fuel burns to completion (Çengel, et Al. 2002). The general form of an equation for complete and stoichiometric combustion is given by (Heywood. 1988).

$$C_aH_b + (a + \frac{b}{4})(O_2 + 3.76N_2) \rightarrow aCO_2 + \frac{b}{2}H_2O + 3.76(a + \frac{b}{4})N_2 \qquad (2.1)$$

The ideal combustion process during which a fuel is burned completely with theoretical air is called the stoichiometric or theoretical combustion of fuel. As it is shown in Equation (2.1), the stoichiometric coefficient f_{stoich} is defined as:

$$f_{stoich} = a + \frac{b}{4} \qquad (2.2)$$

For example for a fuel/air reaction with pure methane (CH_4), the stoichiometric coefficient for air $f_{stoich} = 2$ and the theoretical stoichiometric combustion becomes

$$CH_4 + 2(O_2 + 3.76\,N_2) \rightarrow CO_2 + 2\,H_2O + 7.52\,N_2 \tag{2.3}$$

Notice that the products contain no unburned CH_4 and no C, H_2, CO, NO or free O_2. In an actual combustion processes, it is common practice to use more air than the stoichiometric amount to control the temperature of the combustion chamber. The amount of air in excess of the stoichiometric amount is called excess air. How much air is used in a combustion processes is also expressed in terms of the equivalence ratio ϕ which is defined as:

$$\phi = \frac{FA_{act}}{FA_{stoich}} \tag{2.4}$$

The stoichiometric fuel/air ratio is defined as:

$$FA_{stoich} = \frac{M_f}{f_{stoich}(M_{O_2} + 3.76 M_{N_2})} \tag{2.5}$$

The actual fuel/air ratio can be found from the actual air and fuel mass flow.

$$FA_{act} = \frac{\dot{m}_{f,act}}{\dot{m}_{a,act}} \tag{2.6}$$

With an equivalence ratio of less then one, the combustion mixture is lean on fuel and therefore called lean. If the ratio is more then one, the mixture is called rich because there is insufficient oxygen to completely oxidize the fuel.

As an example, assuming a methane/air mixture with 50% excess air, the combustion reaction becomes

$$CH_4 + 3(O_2 + 3.76\,N_2) \rightarrow CO_2 + 2\,H_2O + O_2 + 11.28\,N_2 \tag{2.7}$$

A methane/air mixture with 50% excess air has an equivalence ratio of 0.666.

Incomplete Combustion Process

The combustion process is incomplete if the combustion products contain any unburned fuel or components such as C, H_2, CO, NO, or OH.

Insufficient oxygen is an obvious reason for incomplete combustion, but it is not the only one. Incomplete combustion occurs even when more oxygen is present in the combustion chamber than it is needed for complete combustion. This may be attributed to insufficient mixing in the combustion chamber during the limited time that the fuel and the oxygen are in contact. Another cause of incomplete combustion is dissociation, where molecules separate or split into smaller molecules. Dissociation becomes important at high temperatures.

Oxygen has a much greater tendency to combine with hydrogen then with carbon. Therefore, hydrogen in fuel normally burns to completion, forming H_2O, even when there is less oxygen than needed for complete combustion. Some of the carbon, however, ends up as CO or just as plain C particles (soot) in the products (Lefebvre. 1999).

Equilibrium

Incomplete combustion occurs because the combustion reactions are frozen before equilibrium completion is reached even when there is sufficient time and oxygen. A system is said to be in equilibrium if no changes occur within the system when it is isolated from the surrounding (Çengel, et al. 2002). The criterion for chemical equilibrium is based on the second law of thermodynamics, and for a system at a specified temperature and pressure, it can be expressed as

$$\left(dG\right)_{T,P} = 0 \tag{2.8}$$

For the reaction

$$\nu_A A + \nu_B B \rightleftarrows \nu_C C + \nu_D D \tag{2.9}$$

where the ν's are the stoichiometric coefficients, the equilibrium criterion can be expressed in terms of the Gibbs function as

$$\nu_C \overline{g}_C + \nu_D \overline{g}_D - \nu_A \overline{g}_A - \nu_B \overline{g}_B = 0 \tag{2.10}$$

This relationship is valid for any chemical reaction regardless of the phases involved. For reacting systems that consist of ideal gases only, the equilibrium constant K_p can be expressed as:

$$K_p = e^{-\Delta G(T)/(R_u T)} \tag{2.11}$$

The standard-state Gibbs function change $\Delta G(T)$ and the equilibrium constant K_p are defined as

$$\Delta G(T) = \nu_C \bar{g}_C(T) + \nu_D \bar{g}_D(T) - \nu_A \bar{g}_A(T) - \nu_B \bar{g}_B(T) \tag{2.12}$$

and

$$K_p = \frac{p_C^{\nu_C} p_D^{\nu_D}}{p_A^{\nu_A} p_B^{\nu_B}} \tag{2.13}$$

Here, p_i's are the partial pressures of the components in atm. The K_p of ideal-gas mixtures can also be expressed in terms of the mole numbers of the components as

$$K_p = \frac{N_C^{\nu_C} N_D^{\nu_D}}{N_A^{\nu_A} N_B^{\nu_B}} \left(\frac{p}{N_{tot}} \right)^{\Delta\nu} \tag{2.14}$$

where

$$\Delta\nu = \nu_C + \nu_D - \nu_A - \nu_B \tag{2.15}$$

The parameter p is the total pressure in atm, and N_{tot} is the total number of moles present in the reaction chamber, including any inert gases. Equation (2.14) is written for a reaction involving two reactants and two products, but it can be extended to several involving a number of reactants and products.

The following example shows the equilibrium calculation of a methane-air mixture at a given temperature and pressure. Equation (2.16) shows the 10 first equilibrium products selected by Ferguson, et al. (2001).

$$\begin{gathered} C_\alpha H_\beta + \frac{f_{stoich}}{\phi}(O_2 + 3.76N_2) \\ \rightarrow \\ n_1 CO_2 + n_2 H_2O + n_3 N_2 + n_4 O_2 + n_5 CO + n_6 H_2 + n_7 H + n_8 O + n_9 OH + n_{10} NO \end{gathered} \tag{2.16}$$

Besides the known reaction for complete combustion, shown in Equation (2.1), six more reaction take place.

$$0.5H_2 \rightleftarrows H \tag{2.17}$$

$$0.5O_2 \rightleftarrows O \tag{2.18}$$

$$0.5O_2 + 0.5N_2 \rightleftarrows NO \tag{2.19}$$

$$0.5H_2 + 0.5O_2 \rightleftarrows OH \tag{2.20}$$

$$H_2 + 0.5O_2 \rightleftarrows H_2O \tag{2.21}$$

$$CO + 0.5O_2 \rightleftarrows CO_2 \tag{2.22}$$

Equation (2.23) expresses the equilibrium constant as a function of temperature T for a variety of reactions. The coefficients A_i, B_i, C_i, D_i and E_i for the Equations (2.17) - (2.22) can be found in Table 2.1.

$$K_{eq}(i,T) = 10^{\left(A_i \cdot \ln\left(\frac{T}{1000}\right) + \frac{B_i}{T} + C_i + D_i \cdot T + E_i \cdot T^2\right)} \tag{2.23}$$

Table 2.1 Equilibrium constant curve-fit coefficients for Equation (2.23).

i	Eq.	A_i	B_i	C_i	D_i	E_i
1	(2.17)	0.432168	-0.112464 x 10^5	2.67269	-0.745744 x 10^{-4}	0.242484 x 10^{-8}
2	(2.18)	0.310805	-0.129540 x 10^5	3.21779	-0.738336 x 10^{-4}	0.344645 x 10^{-8}
3	(2.19)	-0.142784	-0.213308 x 10^4	0.853461	0.355015 x 10^{-4}	-0.310227 x 10^{-8}
4	(2.20)	0.0015079	-0.470959 x 10^4	0.646096	0.272805 x 10^{-5}	-0.154444 x 10^{-8}
5	(2.21)	-0.752364	0.124210 x 10^5	-2.60186	0.259556 x 10^{-3}	-0.162687 x 10^{-7}
6	(2.22)	-0.00415302	0.148627 x 10^5	-4.75746	0.124699 x 10^{-3}	-0.900227 x 10^{-8}

Source: (Ferguson, et al. 2001)

To find the products $n_1 - n_{10}$, the following set of Equations is applied:

H balance: $$\beta = 2n_2 + 2n_6 + n_7 + n_9 \tag{2.24}$$

N balance: $$\frac{f_{stoich}}{\phi} \times 2 \times 3.76 = 2n_3 + n_{10} \tag{2.25}$$

O balance: $$\frac{2f_{stoich}}{\phi} = 2n_4 + n_5 + 2n_1 + n_2 + n_8 + n_9 + n_{10} \tag{2.26}$$

$$N_{tot} = \sum_{i=1}^{10} n_i \tag{2.27}$$

$$K_{eq}(1,T) = \frac{\left(\frac{n_7}{N_{tot}}\right)}{\left(\frac{n_6}{N_{tot}}\right)^{0.5}} \tag{2.28}$$

$$K_{eq}(2,T) = \frac{\left(\frac{n_8}{N_{tot}}\right)}{\left(\frac{n_4}{N_{tot}}\right)^{0.5}} \tag{2.29}$$

$$K_{eq}(3,T) = \frac{\left(\frac{n_9}{N_{tot}}\right)}{\left(\frac{n_4}{N_{tot}}\right)^{0.5}\left(\frac{n_6}{N_{tot}}\right)^{0.5}} \tag{2.30}$$

$$K_{eq}(4,T) = \frac{\left(\frac{n_{10}}{N_{tot}}\right)}{\left(\frac{n_4}{N_{tot}}\right)^{0.5}\left(\frac{n_3}{N_{tot}}\right)^{0.5}} \tag{2.31}$$

$$K_{eq}(5,T) = \frac{\left(\frac{n_2}{N_{tot}}\right)}{\left(\frac{n_4}{N_{tot}}\right)^{0.5}\left(\frac{n_6}{N_{tot}}\right)} \tag{2.32}$$

$$K_{eq}(6,T) = \frac{\left(\frac{n_1}{N_{tot}}\right)}{\left(\frac{n_5}{N_{tot}}\right)\left(\frac{n_4}{N_{tot}}\right)^{0.5}} \tag{2.33}$$

Table 2.2 shows the results of simultaneously solving Equations (2.24) - (2.33) for methane at an equivalence ratio of 0.666 and a temperature of 1,800 Kelvin. The products given by assuming complete combustion, CO_2, H_2O, N_2 and O_2, make 99.7 percent of the equilibrium products.

Table 2.2 Equilibrium products of methane and air at 1,800 Kelvin

Atom	Amount in Mole	Percent	Atom	Amount in Mole	Percent
CO2	0.999233	6.538	H2	0.000431	0.003
H2O	1.995068	13.054	H	3.05×10^{-5}	0.000
N2	11.26188	73.688	O	0.000443	0.003
O2	0.98001	6.412	OH	00891	0.059
CO	0.000767	0.005	NO	0.036271	0.237

Gas Turbine Combustors

All gas turbine combustors perform the same function; they increase the temperature of a high-pressure gas. There are two basic types of combustor designs used for industrial gas turbines, tuboannular and annular. Figure 2-1 shows a tuboannular combustor arrangement. Usually a group from six to ten tubular liners is arranged inside a single annular casing. Drawbacks of this design emerge when trying to achieve a satisfactory and consistent airflow pattern where the design of the diffuser can present serious difficulties (Lefebvre. 1999).

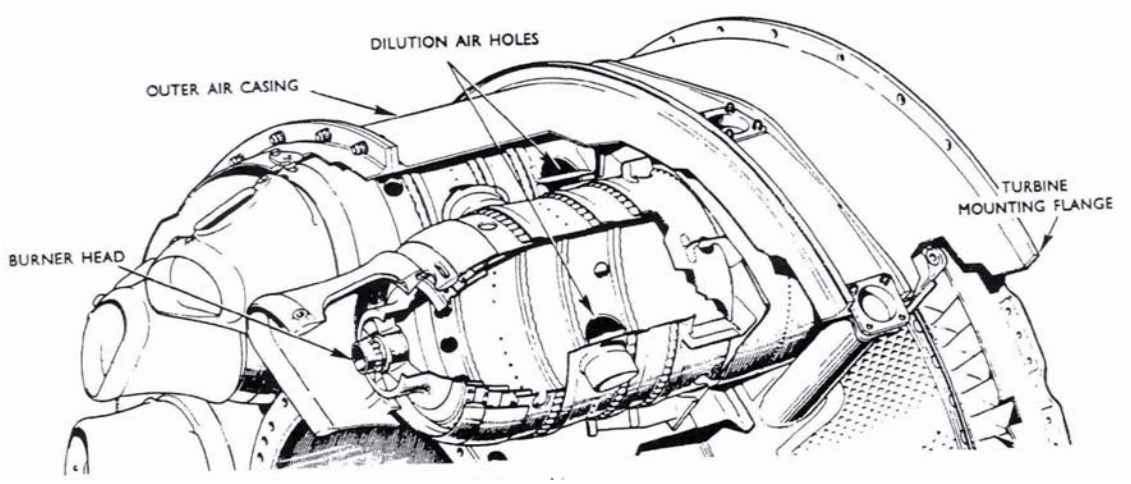

Figure 2-1 Tuboannular combustor arrangement

Source: (Lefebvre. 1999)

Most modern combustors are annular, shown in Figure 2-2. An annular combustor allows a much compacter and lighter architecture, while using the whole volume available in a sector which is larger than a can section. The main drawback is that a tiny local change on the external liner, due to stress or erosion, will have a significant impact on the value of the outlet temperature (Lefebvre. 1999).

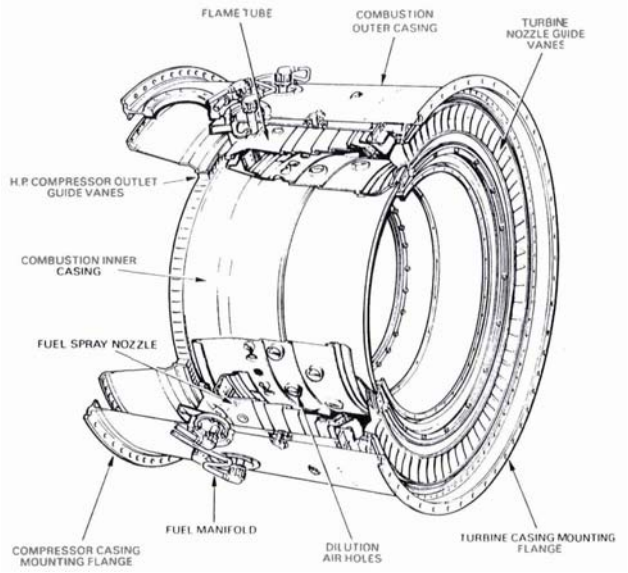

Figure 2-2 Annular combustor

Source: (Lefebvre. 1999)

The pressure drop in a combustor can be mathematically described as:

$$\Delta P = \Delta P_{\text{cold}} + \Delta P_{\text{hot}} \tag{2.34}$$

The cold loss represents the losses arising in the diffuser and the liner at cold flow conditions without the influence of the hot combustion flame. Typical values of cold pressure losses in modern combustors range from 2.5 – 5 percent of the combustor inlet pressure (Lefebvre. 1999).

The fundamental pressure loss that occurs whenever heat is added to a flowing gas is given by:

$$\Delta P_{\text{hot}} = \frac{\rho v^2}{2}\left(\frac{T_4}{T_2} - 1\right) \tag{2.35}$$

The parameter T_2 is the inlet temperature and T_4 is the outlet temperature of the combustor. To reduce the compressor outlet velocity to a value at which the combustor pressure loss is tolerable, it is customary to use a diffuser. The function of the diffuser is not only to reduce the velocity of the combustor inlet air, but also to recover as much of the dynamic pressure as possible and present the liner with a smooth and stable flow. The total pressure loss in a combustor is typically in the range of 3 - 8 percent of total pressure at combustion inlet (Lefebvre. 1999).

Despite many design differences in combustors, all conventional gas turbine combustion chambers have a burning zone, a recirculation zone and a dilution zone, shown in Figure 2-3.

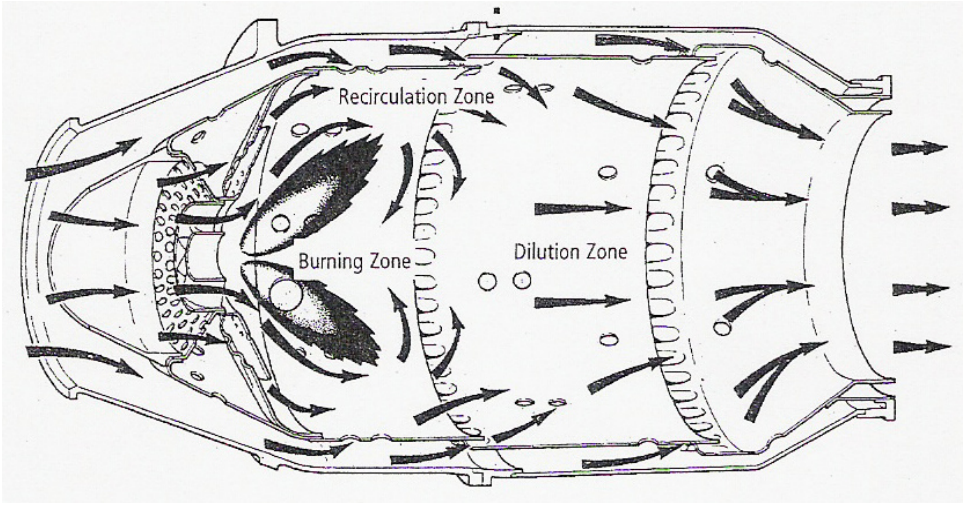

Figure 2-3 Main components of a conventional combustor

Source: (Boyce. 2002)

The main function of the burning zone is to anchor the flame and provide sufficient time, temperature and turbulence to achieve essentially complete combustion of the incoming fuel/air mixture. The function of the recirculation zone is to evaporate (if necessary), partly oxidize, and prepare the fuel for rapid combustion within the remainder of the burning zone. The role of the dilution zone is to admit the remaining air to the combustion mixture to provide an outlet stream with a sufficiently uniform temperature distribution that is acceptable to the turbine.

Dry Low NO_x Combustor

Figure 2-4 shows a schematic of a conventional and lean-premixed combustor. The general idea behind a dry low NO_x (DLN) combustor is to generate a thoroughly mixed lean fuel and air mixture prior to entering the combustor of the gas turbine. The lean mixture creates a relatively low flame temperature, which produces lower amounts of NO_x. Because the mixture is very lean, in fact fairly close to the lean extinction limit, the fuel/air ratio has to be kept constant within narrow limits. This is also necessary due to another constraint. The lower combustion temperature tends to lead to higher concentrations of products related to incomplete combustion, such as CO and unburned hydrocarbons. The necessity to control the fuel/air ratio closely yields different part-load behavior when comparing gas turbines with conventional combustors and DLN engines. At certain levels of part load, DLN engines usually bleed a certain amount of air from the compressor exit directly into the exhaust duct. Therefore, while the airflow for any two shaft engines is reduced at part load, the reduction in airflow is greater for a conventional combustion engine than for a DLN engine (Kurz, et al. 2003). Further explanation about DLN combustors will follow in Chapter 5.

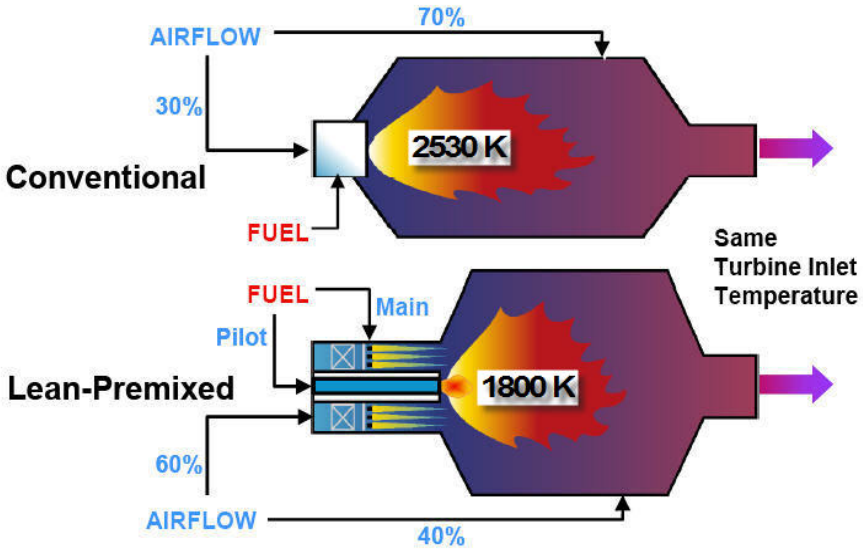

Figure 2-4 Schematic of a conventional and a lean-premixed combustor

Source: (Kurz, et al. 2003)

Emissions

The combustion in a gas turbine is an incomplete process. The exhaust products mainly are carbon dioxide (CO_2), water vapor (H_2O), excess atmospheric oxygen (O_2) and nitrogen (N_2). Carbon dioxide and water vapor have not always been regarded as pollutants because they are the natural consequence of complete combustion of a hydrocarbon fuel. However, they both contribute to global warming and can only be reduced by burning less fuel (Lefebvre. 1999).

For a gas turbine engine burning a lean mixture of natural gas and air, the emissions of unburned hydrocarbons (UHC) and sulfur (SO_x) are negligibly small and therefore most regulations for stationary gas turbines have been directed at oxides of nitrogen and carbon monoxides. In the USA, the Environmental Protection Agency (EPA) has promulgated such emissions standards. Because of growing public awareness, some areas as, for example southern California, set there own much lower emission standards. Depending on the use of the gas turbine and the engine's input energy, typical CO limits range from 10 to 40 ppm. Typical NO_x limits can vary from 10 to 70 ppm. These limits are expressed in parts per million, referenced to 15 percent oxygen on a dry basis. The purpose is partly to remove ambiguity when comparing different sets of experimental data, but also to indicate that combustors burning less fuel are expected to produce less NO_x. The correction formula is given by Lefebvre (Lefebvre. 1999):

$$(NO_X)_{\text{ref 15\% oxygen}} = \frac{5.9\, NO_{X\,\text{meas}}}{20.9 - O_{2\,\text{meas}}} \tag{2.36}$$

The NOx concentrations are expressed in ppm (dry) and O_2 content is expressed in percentage by volume.

The attainment of low CO levels has not presented any major difficulties in the past, due largely to the user's insistence on high combustion efficiencies to minimize fuel consumption. However, the continuing pressure to reduce NO_x emissions has resulted in the adoption of lean, premixed combustion. The success of this technique relies on the lowering of the flame temperature which tends to promote the formation of CO. Thus, the

control of CO now posies a more difficult problem than when the emissions regulations for stationary engines were first formulated (Lefebvre. 1999).

Carbon Monoxide

Carbon monoxide is toxic and harmful to humans. Shown in Figure 2-5, CO reduces the capacity of the blood to absorb oxygen and can cause, in high concentrations, asphyxiation and even death (Turns. 2000).

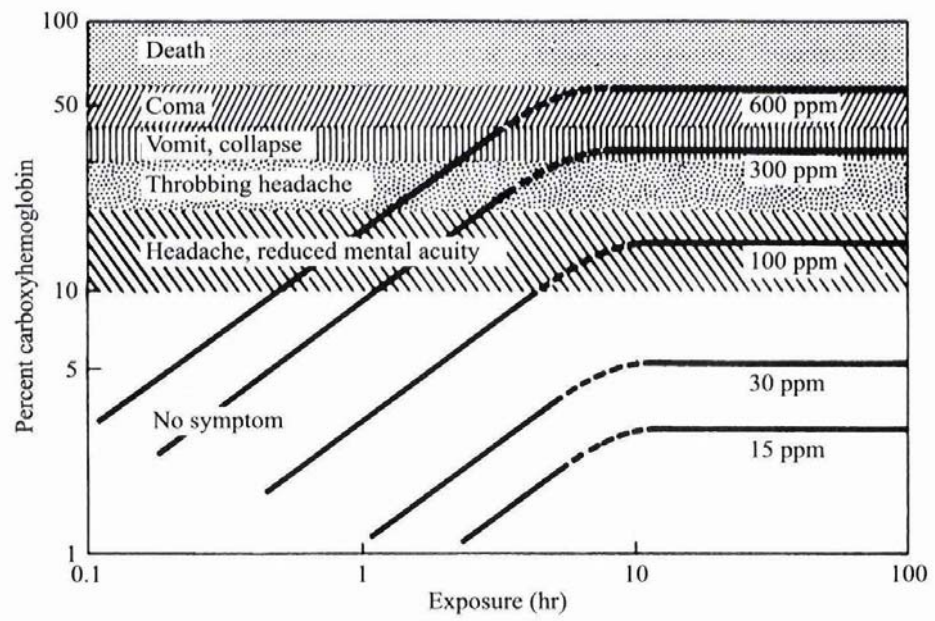

Figure 2-5 Effects of CO exposure on humans

Source: (Turns. 2000)

Large amounts of CO are formed in fuel-rich combustion because of the lack of sufficient oxygen to complete the reaction to CO_2. If the combustion mixture is stoichiometric or moderately fuel–lean, significant amounts of CO will also be present due to the dissociation of CO_2. In gas turbine combustion, CO emissions are found to be much higher than predicted from equilibrium calculations and to be highest at low–power conditions, where burning rates and peak temperatures are relatively low (Lefebvre. 1999).

This is a conflict with the predictions of the equilibrium theory. It is suggested that much of the CO arises from incomplete combustion of the fuel, caused by one or two of the following (Lefebvre. 1999):

- Inadequate burning rates in the primary zone, due to a fuel-to-air ratio that is too low and/or insufficient residence time; and or
- Inadequate mixing of fuel and air, which produces some regions in which the mixture fuel/air is too low to support combustion, and other in which over-rich combustion yields high local concentrations of CO.

Several researchers have investigated the formation of CO in gas turbines. A main factor influencing the CO emissions is the equivalence ratio that relates to the flame temperature. Figure 2-6 shows a high level of CO at lower primary temperature due to a low equivalence ratio. The high CO is due to the slow rates of oxidation associated with a low combustion temperature. Increasing the equivalence ratio raises the combustion flame temperature, which accelerates the rate of oxidation so that CO emissions decline. At a temperature higher than 1,800 Kelvin, the production of CO by chemical dissociation of CO_2 starts to become significant, which increases the CO level again, as shown in Figure 2-6.

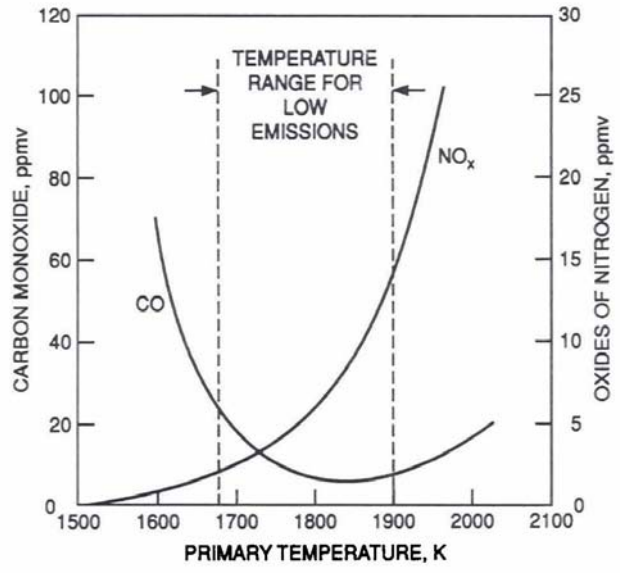

Figure 2-6 Influence of primary-zone temperature on CO and NO_x emissions
Source: (Lefebvre. 1999)

Increasing the pressure also has a beneficial influence on reducing CO emissions. At low temperatures, a higher pressure accelerates the rate of conversion of CO into CO_2. At high temperatures, the CO emissions reduce by suppressing chemical dissociation due to high pressure.

Figure 2-7 shows that a significant amount of CO is formed at the liner wall. The data points of a non air film cooled liner were 500 – 800 ppmv CO lower then the data points of an air film cooled liner at the same conditions. Typically older combustors have a film of cooling air around the liner. The temperature of this air is so low that it freezes the chemical reaction of CO that was formed in the combustion center and has traveled to the wall. This CO will appear in the exhaust unless it reenters back into the hot central core with sufficient time to react to completion. New material developments and new methods of wall cooling that require much less cooling air have lowered the CO emissions.

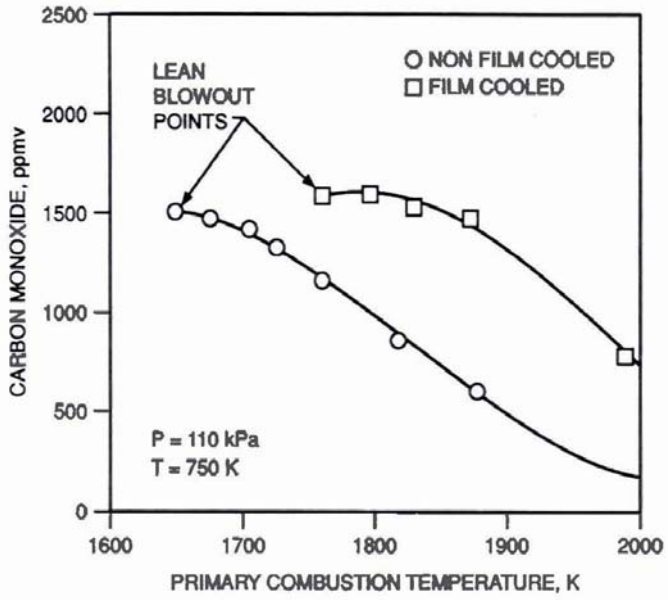

Figure 2-7 Effect of different liner cooling on CO emissions

Source: (Lefebvre. 1999)

Researchers also noticed an influence of the ambient air temperature on CO. Emissions from a 7 MW industrial gas turbine engine supplied with natural gas fuel were 3-4 times higher at a temperature of 287 Kelvin than to the corresponding emissions at 298 Kelvin (Lefebvre. 1999).

Once formed, CO is relatively resistant to oxidation. Under high temperatures the major reaction removing CO is (Lefebvre. 1999):

$$CO + OH \rightleftarrows CO_2 + H \tag{2.37}$$

This is a fast reaction over a broad temperature range. At lower temperatures the reaction becomes (Lefebvre. 1999):

$$CO + H_2O \rightleftarrows CO_2 + H_2 \tag{2.38}$$

CO correlations

Several CO correlations to predict CO emissions in gas turbines were developed by various researchers. The correlation shown in Equation (2.39) was developed by Lefebvre (1984). The relevant temperature is the average temperature in the primary zone T_{pz}, not the peak temperature.

$$CO = \frac{86\dot{m}_a T_{pz} e^{-(0.00345T_{pz})}}{(V_c - V_e)(\frac{\Delta P}{P})^{0.5} P^{1.5}} \tag{2.39}$$

The combustion volume V_c is reduced by the volume employed by the fuel evaporation, obtained as

$$V_e = \frac{0.55\dot{m}_{pz} D_0^2}{\rho_{pz} \lambda_{eff}} \tag{2.40}$$

A comparison between the predicted CO results and the measured emissions showed only small variances over a combustor inlet temperature of 486 – 864 Kelvin.

Rizk, et al. (1993) derived a CO correlation similar to the one from Lefebvre. Their correlation shown in Equation (2.41) depends slightly higher on pressure and lower on combustion temperature. Their correlation was compared to test data with a inlet temperature of 460 – 680 Kelvin.

$$CO = \frac{0.18\times10^9 e^{(\frac{7800}{T_{pz}})}}{P^2(t - 0.4t_e)(\frac{\Delta P}{P})^{0.5}} \tag{2.41}$$

Both correlations were developed for aircraft engines and have to be adjusted for lean premixed industrial gas turbine combustors.

Oxides of Nitrogen

Oxides of Nitrogen, combined with unburned hydrocarbons, form photochemical smog. Particulate matter, also called soot or smoke, creates problems of exhaust visibility and soiling of the atmosphere. It is not normally considered to be toxic at the levels emitted, but recent studies indicate a strong association between asthma and other respiratory diseases. Smog also causes damage to plant life and adds to the problem of acid rain (Lefebvre. 1999).

NO_x Formation Processes

"NO_x" refers to the sum of NO (nitric oxide) and NO_2 (nitrogen dioxide). The formation of NO_2 results only from the oxidation of NO, so the total NO_x (NO + NO_2) is not affected by the amount of NO_2 formed. Therefore, the calculation of NO is normally sufficient for determining NO_x. The remainder of this section will refer only to NO formation.

There are four well-recognized chemical mechanisms for NO formation. These include the Zeldovich, prompt, nitrous oxide, and fuel-bound nitrogen pathways. The following sections provide a description of these four NO producing chemical mechanisms.

Zeldovich Mechanism

The extended Zeldovich mechanism consists of two chain reactions (Turns. 2000):

$$O + N_2 \rightleftarrows NO + N \tag{2.42}$$

$$N + O_2 \rightleftarrows NO + O \tag{2.43}$$

These reactions can be further extended by adding the reaction

$$N + OH \rightleftarrows NO + H \tag{2.44}$$

The NO formed through this mechanism is referred to as thermal NO because the formation rates are only significant at high temperatures (~1,800+ Kelvin) (Turns. 2000). This set of reactions is the most widely used and recognized mechanism for NO formation.

Reaction (2.43) is much faster than reaction (2.42), so the N atom can be assumed to be in steady state. In addition, the NO formation process is assumed to be much slower than the combustion process; this allows the assumption that the elements affecting the formation of NO are in their equilibrium concentrations (Heywood. 1988). With these assumptions, the rate of NO formation becomes:

$$\frac{d[\mathrm{NO}]}{dt} = \frac{2R_1\left\{1-\left([\mathrm{NO}]/[\mathrm{NO}]_e\right)^2\right\}}{1+\left([\mathrm{NO}]/[\mathrm{NO}]_e\right)R_1/\left(R_2+R_3\right)} \tag{2.45}$$

The R_i parameters are based on the forward kinetic reaction rate constants for the three reactions in the extended Zeldovich mechanism [Equations (2.46) - (2.48)] and the equilibrium concentrations of the applicable species:

$$R_1 = k_1^+ [\mathrm{O}]_e [\mathrm{N}_2]_e \tag{2.46}$$

$$R_2 = k_2^+ [\mathrm{N}]_e [\mathrm{O}_2]_e \tag{2.47}$$

$$R_3 = k_3^+ [\mathrm{N}]_e [\mathrm{OH}]_e \tag{2.48}$$

The kinetic rate constants are based on the temperature of the reacting mixture and are readily available for each reaction in the extended Zeldovich mechanism (Heywood. 1988). Equation (2.45) is a simple expression that can be used to calculate the NO formation rate when the temperature and equilibrium concentrations of the applicable species are known.

Prompt Mechanism

The prompt, or Fenimore mechanism, was first proposed by Fenimore in 1971 to account for NO formation that occurred very quickly in the primary reaction zone of the combustor (Fenimore et al. 1971). It was later found that the NO is formed from hydrocarbon fragments present during the combustion process reacting with nitrogen (Nicol et al. 1995). The primary initiating reaction is:

$$\mathrm{N}_2 + \mathrm{CH} \rightleftharpoons \mathrm{HCN} + \mathrm{N} \tag{2.49}$$

The N atom becomes NO through the last two reactions in the Zeldovich mechanism. The HCN route to NO is complex, but its main path is through NCO, NH, N, and then finally to NO through the same Zeldovich N atom reactions.

Fuel-Bound Nitrogen Mechanism

Gas turbines which run on fuel containing nitrogen show an increase in NO production (Toof. 1985). This increase in NO is a result of the conversion of the nitrogen in the fuel to NO. The mechanism begins with the pyrolysis of the nitrogen containing fuel to HCN. The HCN then follows the same pathway to NO as the prompt mechanism. Because of this, the fuel and prompt NO are considered linked processes (Toof. 1985). This mechanism is obviously unimportant in fuels containing no nitrogen, such as natural gas, but contributes significantly when burning nitrogen containing fuels such as coal.

Nitrous Oxide Mechanism

The nitrous oxide (N_2O) mechanism was recognized by Malte and Pratt in 1974 as an important NO pathway (Corr, et al. 1991). It is regarded as being most important in fuel-lean ($\phi < 0.8$), low-temperature conditions, such as those experienced in lean-premixed combustion (Turns. 2000). The three main steps of this mechanism are:

$$O + N_2 + M \rightleftharpoons N_2O + M \tag{2.50}$$

$$H + N_2O \rightleftharpoons NO + NH \tag{2.51}$$

$$O + N_2O \rightleftharpoons NO + NO \tag{2.52}$$

Relative Contributions of Each Mechanism

There are several publications by various authors that analyze the relative contribution of each NO_x mechanism for different fuels, conditions, and combustion types. Most of these studies involve the analysis of lean-premixed combustion because of its popularity as a NO_x reduction strategy.

Correa et al. (1991) performed a number of experiments and numerical simulations to determine the relative contributions of the thermal, nitrous oxide, and prompt NO mechanisms. An early study (Leonard et al. 1990) used experimental NO_x data taken from turbulent, premixed methane-air flames using a perforated-plate burner and compared these data to results from a numerical modeling study which used a well-stirred reactor (WSR) followed by a plug flow reactor (PFR) combined with a kinetic scheme including the Zeldovich and prompt mechanisms. The results of the study

showed that the prompt mechanism dominates below a flame temperature of about 1,800 Kelvin. The study also concluded that NO varies as $\sqrt{p}$ in near-stoichiometric premixed flames, but is independent of pressure in flames below an equivalence ratio of about 0.75. Another pure numerical study was performed for premixed laminar methane-air flames under various conditions (Corr et al. 1991). This study used the Miller-Bowman mechanism for methane combustion and NO formation, which includes the Zeldovich, prompt, and now also the nitrous oxide NO mechanisms (Miller et al. 1989). The study also concluded that thermal NO_x dominated in the near-stoichiometric flames, but that the nitrous oxide mechanism is predominant in lean-premixed, laminar flames. The absence of pressure dependence in very lean flames was also confirmed.

In 1991, Corr et al. presented results from experiments conducted at the University of Washington using a jet-stirred reactor operating at atmospheric pressure that was fired with ethylene and methane using premixed and non-premixed flames. Both NO and NO_2 were measured, and the contribution of each mechanism was deduced from the calculated free radical concentration that would be required to produce the measured NO_x. Both the Zeldovich and nitrous oxide mechanisms rely on the O atom radical for initiation of the reactions, while the prompt mechanism requires the CH radical. The study concluded that unreasonable O atom concentrations would be necessary for the NO_x to be formed by either the Zeldovich or nitrous oxide mechanisms, but that the CH concentrations were reasonable, based on an accompanying numerical study using select reactions from the Miller-Bowman mechanism. Because of this, it was concluded that the prompt NO mechanism was dominant.

Later work done by Nicol et al. (1995), also at the University of Washington, indicates that the nitrous oxide and Zeldovich mechanisms are equally important in high-pressure lean-premixed methane combustion, while the prompt mechanism is practically negligible. Modeling was performed using a WSR to represent the flame zone and a PFR for the post-flame zone. Three different kinetic mechanisms, including the previously mentioned Miller-Bowman scheme, were used, and all showed similar trends. The modeling efforts were verified from porous-plate burner experiments. The result also indicates that for temperatures, pressures, and equivalence ratios capable of producing

NO less than 10 ppmv, the relative contribution of the nitrous oxide mechanism increases steeply and approaches 100 percent. However, for atmospheric combustion, all three pathways contribute similar amounts, and none can be dismissed.

These conclusions differ from the earlier ones of Corr et al. (1991) in that the prompt mechanism is the most dominant. The discrepancy may be because the Corr study used only select reactions from the Miller-Bowman mechanism, which caused the scheme to neglect the super-equilibrium concentration possibilities for the O and OH atoms. These super-equilibrium concentrations can exist at up to 1000 times the equilibrium concentrations in flame regions (Turns. 2000), and this high concentration possibility could perhaps accommodate the high O atom requirement calculated in their study to produce the measured NO_x from the Zeldovich or nitrous oxide mechanisms. This type of NO formation is sometimes linked to the prompt mechanism because it takes place early in the flame front, but the pathway is still that of the Zeldovich mechanism (Turns. 2000).

The conclusions drawn from the review of these studies is that the Zeldovich and nitrous oxide mechanisms are the most important for lean-premixed combustion at gas turbine operating conditions, while the prompt mechanism makes insignificant contributions. These results are largely based on combustor modeling using the most accepted chemical kinetic mechanisms available. In addition, the most accurate method for NO calculation uses a complete kinetic scheme that models both the combustion process and nitric oxide formation.

Current PEMS Technology

The literature review of current PEMS technologies revealed a significant amount of work that has been done to develop PEMS for gas turbines. The bulk of this work was done by W.S.Y. Hung for Solar. All of the previously developed PEMS were primarily based on statistical analysis of CEMS data, not fundamental engineering principles.

PEMS Development by W.S.Y. Hung

W.S.Y. Hung first published 1975 a description of an analytical model used to determine NO_x emissions for a specific family of conventional gas turbine combustors (Hung. 1975a). Shortly after, he published a description of modifications made to the model to include the effects of water injection, operation at reduced air/fuel ratio, primary air leaning, fuel with low flame temperatures, and fuel/air premixing (Hung. 1975b). Because the main feature of this model was the way in which the diffusion process was modeled, it was later referred to as the diffusion-limited mixing model (Hung. 1991). The model showed good agreement with laboratory and field data, but at that time it was only used as a design tool for NO_x reduction in combustors.

Beginning in 1991, Hung published work on a PEMS in which the diffusion-limited mixing model was referenced, but not directly used (Hung. 1991). Instead, the PEMS was based on a performance/emissions program that was developed for various gas turbine models using field data on NO_x emissions. The program was basically developed by gathering NO_x data, correcting it to ISO conditions (using either EPA correlations or special expressions developed by Hung), and establishing the ISO corrected NO_x as functions of fuel/air ratio and water/fuel ratio (if applicable) (Hung, et al. 1995). User inputs of fuel type, duct losses, elevation, combustion system, humidity, and water injection schedule are used to calculate ISO corrected NO_x as a function of ambient temperature and either power turbine inlet temperature (T_5) or gas producer speed. These two functions are stored in the PEMS and used to calculate NO_x based on inputs of those two parameters from the gas turbine control system. The calculated NO_x is then corrected to ambient pressure and humidity using the same correlations used in the development of the performance/emissions program. The diffusion-limited mixing model

was used to verify the performance/emissions program, but no results of this verification were provided (Hung, et al. 1995).

At the end of 1994, Hung reported that 36 PEMS were installed on various SOLAR gas turbines using conventional combustion, water injection, and "SoLoNOx" (Solar's version of lean-premixed) combustion. The relative accuracy ranged from about 2 to 12% when compared to CEMS measurements (Hung, et al. 1995). However, because of problems with the correlations, the end-users removed most, if not all, of these PEMS.

Other PEMS Development

An interesting paper on PEMS development was published in 1997 by Marshall and Bautista (Marshall, et al. 1997). The goal of their project was to develop CO and NO_x emission algorithms for small (< 20 MW) stationary gas turbines used in natural gas pipeline compression stations. The general forms of the NO_x and CO predictive algorithms were based on first engineering principles, but the forms of these algorithms were said to be proprietary and no details of how these algorithms were developed was described in the paper. The coefficients for these algorithms were determined based on regression analysis of data gathered with a CEMS.

The analysis was completed on data from GE Frame 3 and Rolls Royce Avon turbines so that the technique employed could be validated on engines representing old (Frame 3) and recent (Avon) technologies. The data was taken over a wide range of operating conditions and divided into a development subset and a validation subset. The coefficients and applicable operating parameters for the predictive algorithms were determined by using regression analysis on the development subset. The algorithms used parameters such as humidity, ambient temperature, exhaust gas temperature, and gas generator speed, which are all routinely monitored for process control. These applicable operating parameters were then used from the development subset to generate NO_x and CO data to be compared to the validation subset. Relative accuracy for the NO_x data varied between 3 and 5%.

While the results of this work are promising, neither additional publications referencing the continued development of this technique, nor publications describing the application of these algorithms to a field-installed PEMS could be found.

A pure statistical based PEMS was developed by CMC Solutions and the result of their work was published in 2003. Their PEMS uses historical CEMS data to generate predicted emission rates. The PEMS was installed on two GE Frame 7 gas turbines which are operated in a power plant. One of the turbines was a peaking unit burning natural gas and utilizing a DLN (dry low-NOx) combustor, while the other was a base-load unit firing natural gas and/or fuel oil and utilizing steam injection for NOx reduction. The PEMS algorithm was generated using an initial 40 or 60 hours of data gathered by a CEMS. Details of the algorithm development were not provided. The final PEMS algorithm was based on an additional 720 hours of data that was gathered during the demonstration period. This type of PEMS differs from the work presented in this research in that the models are not based on the fundamental physical processes controlling NO_x production.

In addition to the direct PEMS development, a number of semi-analytical expressions have been developed to determine NO_x emissions from gas turbines. In 1981, Lewis published expressions for NO_x prediction on experimental flame data published by NASA (Lewis. 1981).

$$NO_x = 7.50 \times 10^{-6} e^{8.28 \times 10^{-3} T} \tag{2.53}$$

This main expression is only a function of flame temperature, but there are accompanying expressions for correcting this temperature based on humidity, fuel type, power, and water injection. Lewis notes that these correlations are only useful as a design tool. A correlation Lewis published ten years later did include pressure (Lewis. 1991).

$$NO_x = 3.32 \times 10^{-6} \exp(0.008T) P^{0.5} \tag{2.54}$$

Equation (2.54) is intended to show the amount of NO_x formed in lean, homogeneous combustion. It suggests that NO_x formation depends only on the post combustion temperature and pressure and is completely independent of the residence time of the gases in the combustor. According to Lewis, this is because the relevant time is not the residence time of the combustion products, but rater the relaxation time of the molecules involved, primarily the nitrogen molecule, and thus, is the same in all combustion systems using air.

In 1994, Becker and Perkavec published a summary of four equations for NOx emission prediction (Becker, et al. 1994). All of these equations make use of a different set of parameters and constants that were found by fitting equations to experimental or field data. The parameters include fuel/air ratio (or equivalence ratio), combustion pressure, combustion temperature, humidity, and air mass flow rate. The authors state that the four equations are limited to the gas turbine model, operating conditions, and type of fuel used at the time of the equation development. Because of this, a new semi-analytical equation was developed with a minimum number of constants that need to be determined for each combustor and environment it is applicable to. The expression is semi-analytical because it is based on a combustor energy balance used to calculate the flame temperature, but the dependence on NO_x is still found by statistically analyzing the test data. The published comparison between the expression and experimental data is very good for some combustors/fuels while not so good for others. Although it was concluded that the developed expression is effective, there are no published results of an actual PEMS installation using the correlation.

A similar paper was published in 1995 by Bakken and Skogly (Bakken, et al. 1995). Two previously developed correlations are presented, along with a new one:

$$\mathrm{NO}_x = 62\, P^{0.5} FA^{1.4} \exp\left(\frac{-635}{T_4}\right) \tag{2.55}$$

T_4 is the combustor discharge temperature, FA is the fuel/air ratio, and P is the compressor discharge pressure. The new correlation was developed to include the effects of component degradation. Based on their statistical analysis, the effects of component degradation can be captured by measuring only the compressor discharge pressure, fuel/air ratio, and combustor discharge temperature. The correlation presented was implemented in the condition monitoring system of a Sleipner A installation, but the results of this were never published.

An other promising correlation was developed by Rokke et al. (1993)

$$NO_x = 18.1 P^{1.42} \dot{m}_a^{0.3} FA^{0.72} \quad (2.56)$$

Equation (2.56) was found to very satisfactorily correlate measurements of NO_x emissions from five different natural gas-fired industrial machines operating in the power range from 1.5 to 34 MW. Although combustion temperature is conspicuous by its absence in Equation (2.56), its influence on NO_x emissions is acknowledged by the inclusion of a fuel/air ratio term.

Summary Literature Review

Nearly every gas turbine manufacturer uses some form of a lean-premixed gas turbine combustor, also called dry low NO_x combustor, for their gas turbine engines (Lefebvre. 1999). That makes DLN currently the most widely used combustor design method for reducing NO_x and CO emissions in gas turbines. The NO_x formation in a lean-premixed combustion system at gas turbine operating conditions mainly depends on the Zeldovich mechanism (also referred as thermal NO_x) and the nitrous oxide mechanism. The main factors influencing CO emissions are engine and combustor inlet temperatures, combustion pressure and primary-zone equivalence ratio (Lefebvre. 1999).

CO and NO_x emissions are harmful to humans and environment. The responsible regulatory agencies often require some sort of emissions monitoring systems. Instead of using a continuous emissions monitoring system (CEMS), a parametric emissions monitoring system (PEMS) has potential economic and technical advantages. Various researchers developed different PEMS models based on fundamental physical processes or pure statistical analysis of measured emissions data. Although most results were promising, PEMS has not been widely established yet within the natural gas transmission industry.

CHAPTER 3 - Mathematical Model

Figure 3-1 shows a schematic of a two shaft industrial gas turbine with a dry low NO_x (DLN) combustor. Typical control systems for such a gas turbine measure the ambient conditions, speed of compressor and turbine, air and fuel flows and sometimes the temperature T_5 between the gas producer turbine and power turbine.

NO_x and CO emissions in a gas turbine are a function of the combustion temperatures, pressures and mass flows. Unfortunately, most gas turbine control systems do not measure the inlet, inside and outlet of the combustor. A successful mathematical model used in PEMS must calculate these parameters as accurately as possible .This Chapter describes the engineering principles used in the developed gas turbine combustor model, specifically focusing on stations 2, 3 and 4 in Figure 3-1. The development of the remaining equations yielding the complete set of modeling equations is given in this Chapter. These modeling equations are based on fundamental thermodynamic and stoichiometric principles that describe the gas turbine system.

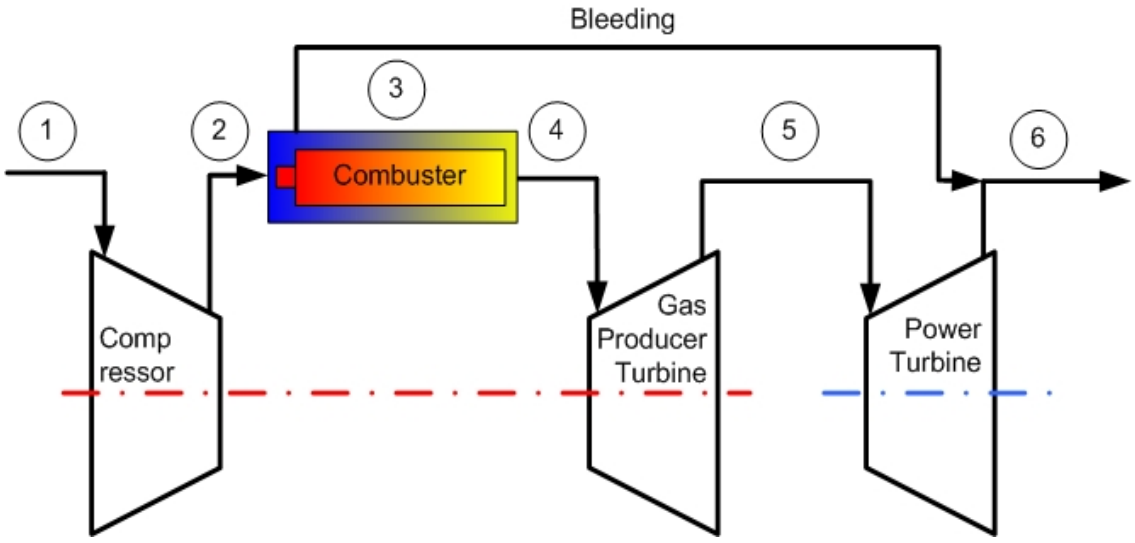

Figure 3-1 Schematic of a two shaft gas turbine with bleed valve

Description of Combustor Modeling Layout

Previously discussed studies on emission formation modeled the combustor with a well-stirred reactor (WSR), sometimes called perfectly-stirred reactor (PSR), for flame stabilization, followed by a plug-flow reactor (PFR). A WSR is a one-dimensional control volume in which perfect instantaneous mixing of all species is assumed. The control volume is also assumed to have uniform temperature and pressure, and the gaseous species are assumed to behave as ideal gases. A PFR represents an ideal reactor in steady-state with steady-flow. It is also assumed that there is no mixing in the axial (or flow) direction, and that the mixture properties are uniform in the radial direction. Ideal frictionless flow and ideal gas behavior is also assumed.

The combustor model developed in this research uses a lean-premixed combustion system for natural gas. Figure 3-2 illustrates the model that is developed with a series of PFR's which represent the combustion zones. Outside and concentric to this is another series of PFR's that represent the combustion liner cooling air. The model requires knowledge of combustion air to cooling air ratio, velocities through the combustor, geometry of the combustor, and the combustor temperature profile.

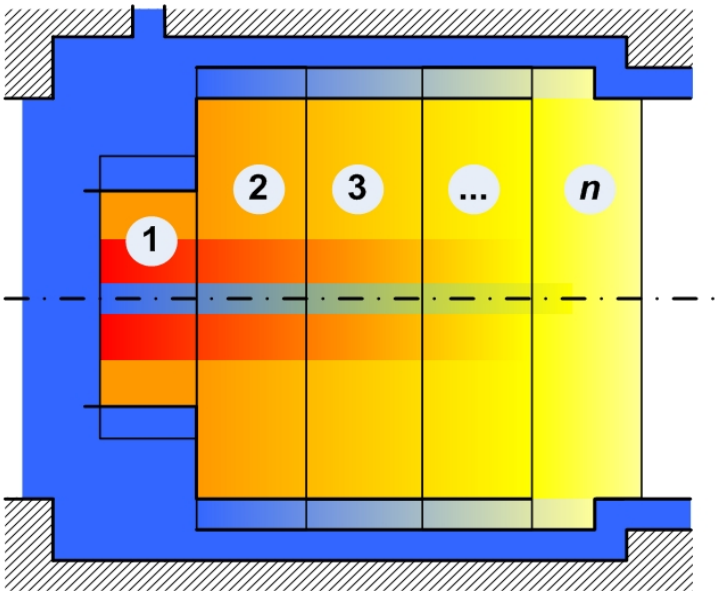

Figure 3-2 Model with consecutive PFR's

A graphical representation of the model is shown in Figure 3-3. As shown, the mass flow of air and fuel is divided into several sections:

A	Center air	D	Cooling air combustion
B	Pilot burner	E	Cooling air turbine
C	Main combustion	F	Bleeding air

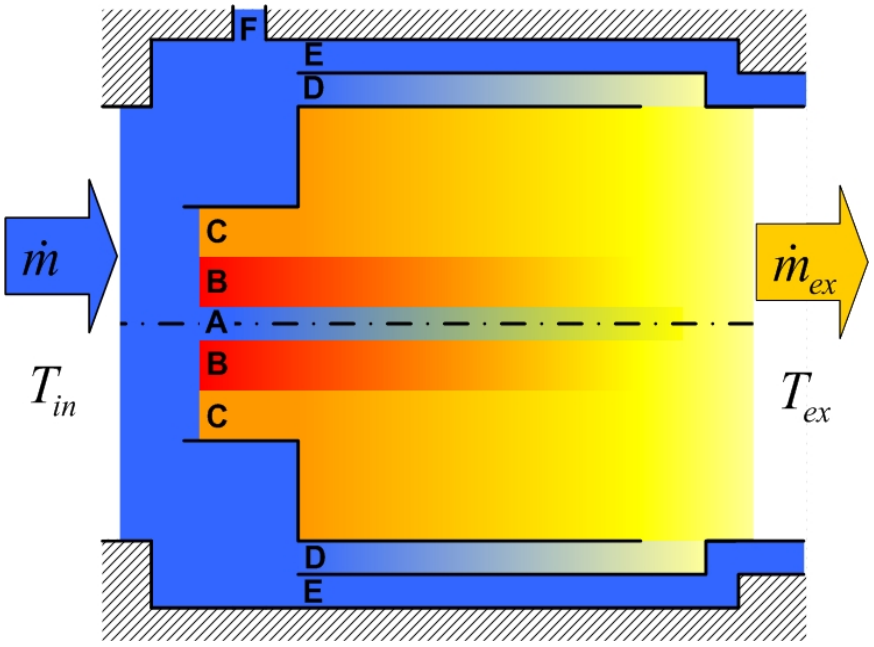

Figure 3-3 Schematic of the combustor model

The combustor inlet energy can be calculated from the input temperature T_{in} and the mass flow of air and fuel:

$$\dot{E}_{in} = T_{in}\left(c_{p,a} \sum_{i=A}^{F} \dot{m}_{i,a} + c_{p,f} \sum_{i=B}^{C} \dot{m}_{i,f} \right) + LHV \sum_{i=B}^{C} \dot{m}_{i,f} \tag{3.1}$$

The output energy is given by the exhaust, bleeding and turbine cooling air:

$$\dot{E}_{out} = T_F\, c_{p,a}\, \dot{m}_{F,a} + T_E\, c_{p,a}\, \dot{m}_{E,a} + T_{ex}\, c_{p,ex}\, \dot{m}_{ex} \tag{3.2}$$

The system is assumed to be adiabatic, and there is no heat transfer between the turbine cooling air and the combustor cooling air. Where solved, these equations provide the temperature field throughout the combustion system. The following sub-sections describe the additional mathematical models necessary to solve Equation (3.1) and (3.2).

Combustion Inlet Conditions

The combustor inlet temperature and pressure is calculated based on the ambient conditions, compressor pressure ratio, and the compressor isentropic efficiency. The isentropic temperature $T_{2,s}$ is

$$T_{2,s} = T_{amb}\left(PR\right)^{\frac{\gamma-1}{\gamma}} \tag{3.3}$$

The actual temperature T_{in} is determined from the isentropic efficiency as stated

$$T_2 = \frac{T_{2,s} - T_{amb}}{\eta_{s,comp}} + T_{amb} \tag{3.4}$$

Knowing the input temperature, the compressor work is determined from the relation:

$$w_{Comp} = \frac{c_{p,a\,T_{amb}} + c_{p,a\,T_2}}{2}\left(T_{amb} - T_2\right) \tag{3.5}$$

Zone-by-Zone Combustion Analysis

The actual model is divided into several zones with different combustion in each zone. The combustor model in Figure 3-4 shows one zone where the combustion gas temperature is calculated. For better visualization and because of symmetry just the upper half of the model is shown.

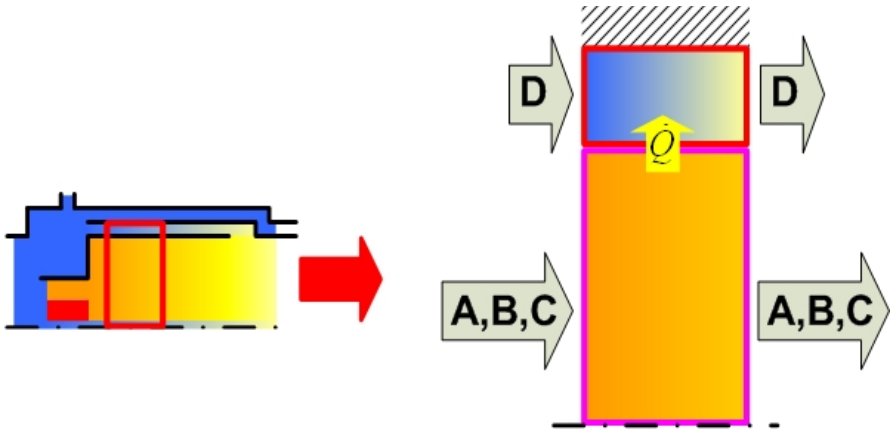

Figure 3-4 Combustion zone

The energy inputs for a zone are given by Equation(3.6) and Equation(3.7).

$$\dot{E}_{D,in} = T_{D,in}\, c_{p,a}\, \dot{m}_D \tag{3.6}$$

$$\dot{E}_{ABC,in} = T_{ABC,in}\, c_{p,ABC}\, \dot{m}_{ABC} \tag{3.7}$$

To find the combustion and cooling air temperature, a set of five equations with five unknowns is used:

$$\dot{Q} = h\, A (T_{ABC,out} - T_{D,out}) \tag{3.8}$$

$$\dot{E}_{D,out} = T_{D,out}\, c_{p,a}\, \dot{m}_D \tag{3.9}$$

$$\dot{E}_{D,in} + \dot{Q} = \dot{E}_{D,out} \tag{3.10}$$

$$\dot{E}_{ABC,out} = T_{ABC,out}\, c_{p,ABC}\, \dot{m}_{ABC} \tag{3.11}$$

$$\dot{E}_{ABC,in} - \dot{Q} = \dot{E}_{ABC,out} \tag{3.12}$$

The heat transfer coefficient *h* can be calculated by a set of equations described in the heat transfer section late in this chapter.

Assuming the primary zone is divided into three zones. In the first characteristics zone, 100 percent of the pilot fuel/air and 20 percent of the main fuel/air mixture burns. The remaining 80 percent of the main fuel/air mixture burns in the second zone and no combustion occurs in the third zone. The input and output energy $\dot{E}_{ABC}$ calculated in Equation(3.7) and (3.11) now is split into $\dot{E}_A$, $\dot{E}_B$ and $\dot{E}_C$.

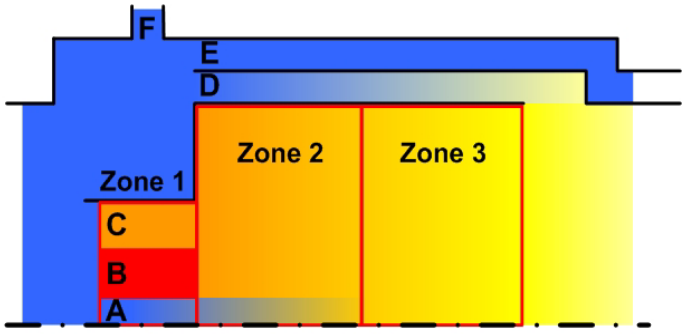

Figure 3-5 Model with 3 combustion zones

Looking at zone 2, the mass flow of the center air, shown by the index A, will not change. The inlet air and outlet air remains the same.

$$\dot{E}_{A,in} = T_{A,in} c_{p,a} \dot{m}_A \tag{3.13}$$

$$\dot{E}_{A,out} = T_{A,out} c_{p,a} \dot{m}_A \tag{3.14}$$

For the pilot burner section B, only exhaust enters the second zone, since it is assumed that the pilot combustion is complete in the first zone. That gives the following input and output energies

$$\dot{E}_{B,in} = T_{B,in} c_{p,ex\,pilot} \dot{m}_B \tag{3.15}$$

$$\dot{E}_{B,out} = T_{B,out} c_{p,ex\,pilot} \dot{m}_B \tag{3.16}$$

The mass flow $\dot{m}_B$ is the summation of pilot air and pilot fuel. The most significant change is in the main burner section. At the inlet 20 percent is exhaust and 80 percent is fuel and air, which will turn into 100 percent exhaust at the outlet. The energy balance for the main burner section C becomes:

$$\dot{E}_{C,in} = T_{C,in} \left[Zr_C \left(c_{p,a} \dot{m}_{C,a} + c_{p,f} \dot{m}_{C,f} \right) + Zp_C \, c_{p,ex} \dot{m}_C \right] + Zr_C \, LHV \, \dot{m}_{C,f} \tag{3.17}$$

$$\dot{E}_{C,out} = T_{C,out} c_{p,ex\,main} \, \dot{m}_C \tag{3.18}$$

The coefficient Zr_C, which varies between 0 and 1, represents the reactants of air and fuel entering the zone. The corresponding coefficient Zp_C represents the products. In this example $Zr_C = 0.8$ and $Zp_C = 0.2$.

Chemical Reaction

The constituents of air are assumed as oxygen, nitrogen and water vapor. The amount of water vapor is given by the relative humidity. The fuel, which is assumed to be pure methane (CH_4), is allowed to partially react in each zone. This leads to the following chemical relationship for stoichiometric or lean complete combustion:

$$a_{CH_4}CH_4 + a_{O_2}O_2 + a_{N_2}N_2 + a_{H_2O}H_2O + a_{CO_2}CO_2 \longrightarrow b_{CO_2}CO_2 + b_{H_2O}H_2O + b_{O_2}O_2 + b_{N_2}N_2 + b_{CH_4}CH_4 \tag{3.19}$$

The mass balance is made for 1mol of CH_4. The equivalence ratio ϕ and the stoichiometric coefficient f_{stoich} are given by Equations (2.2) and (2.4). The reactants a are found with the following relations:

$$a_{CH_4} = 1 \tag{3.20}$$

$$a_{O_2} = \frac{f_{stoich}}{\phi} \tag{3.21}$$

$$a_{N_2} = \frac{f_{stoich}\,3.76}{\phi} \tag{3.22}$$

$$a_{H_2O} = a_{O_2}\,1.608\,\frac{0.622\,P_{sat}\,RH}{P_{atm}} \tag{3.23}$$

The reactant a_{CO_2} for CO_2 is set to zero for the first zone.

The following products are defined assuming a stoichiometric or lean fuel-to-air mixture.

$$b_{CO_2} = a_{CH_4} + a_{CO_2} \tag{3.24}$$

$$b_{H_2O} = a_{H_2O} + f_{stoich} \tag{3.25}$$

$$b_{N_2} = a_{N_2} \tag{3.26}$$

$$b_{O_2} = a_{O_2} - f_{stoich} \tag{3.27}$$

Because complete combustion is assumed for the model, b_{CH_4} equals zero at the outlet of the combustor.

Exhaust c_p

Knowing the products of the combustion mixture, the exhaust $\overline{c}_p$ value is then found by:

$$\overline{c}_{p,ex} = \frac{b_{\mathrm{CO_2}}\,\overline{c}_{p,\mathrm{CO_2}} + b_{\mathrm{H_2O}}\,\overline{c}_{p,\mathrm{H_2O}} + b_{\mathrm{N_2}}\,\overline{c}_{p,\mathrm{N2}} + b_{\mathrm{O_2}}\,\overline{c}_{p,\mathrm{O2}}}{b_{\mathrm{CO_2}} + b_{\mathrm{H_2O}} + b_{\mathrm{N_2}} + b_{\mathrm{O_2}}} \tag{3.28}$$

Of course, Equation (3.28) just shows the exhaust c_p for one axial zone. The exhaust c_p for the main burner will be different from the pilot burner.

To calculate the overall exhaust c_p shown in Figure 3-3, all axial sections plus the combustor cooling air section has to be considered.

$$c_{p,ex} = \frac{\dot{m}_A\,c_{p,air\,A} + \dot{m}_B\,c_{p,ex\,B} + \dot{m}_C\,c_{p,ex\,C} + \dot{m}_D\,c_{p,air\,D}}{\dot{m}_A + \dot{m}_B + \dot{m}_C + \dot{m}_D} \tag{3.29}$$

Gas Producer Turbine

By necessity, the work of the compressor equals the work of the gas producer turbine,

$$w_{Comp} = w_{GPT} \tag{3.30}$$

The gas producer turbine outlet temperature T_{GPT} is then calculated by

$$T_{GPT} = T_{ex} - \frac{w_{GPT}}{c_{p,ex}} \tag{3.31}$$

T_{GPT} is often measured in gas turbine control systems.

Heat Transfer

The heat transfer between combustion and cooling air is assumed to be the same as an uncooled liner-wall example given by Lefebvre (1999). The liner is heated by radiation and convection from the hot gases inside and is cooled by radiation to the outer casing and by convection to the annulus cooling air outside. The heat transfer model shown in Figure 3-6 includes only the axial variation of radiation and convection. Radiation and convection is assumed to be constant around the circumference at any axial location.

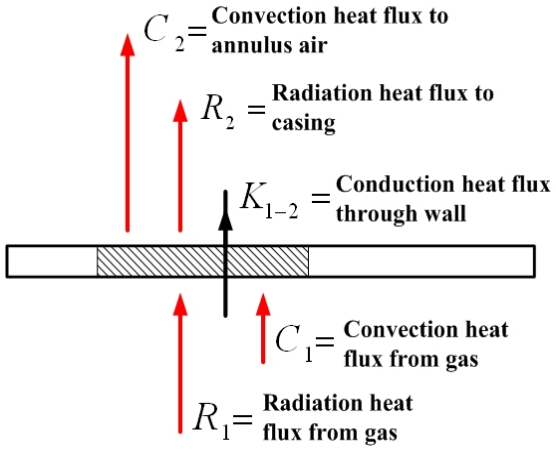

Figure 3-6 Basic heat-transfer processes

Under steady-state conditions, Figure 3-6 shows that the rate of heat transfer into a wall element must be balanced by the rate of heat transfer out

$$R_1 + C_1 = R_2 + C_2 = K_{1-2} \tag{3.32}$$

Equation (3.32) assumes a thin liner wall, such that

$$\Delta A_{w1} \cong \Delta A_{w2} \tag{3.33}$$

K_{1-2} is the conduction heat transfer rate through a solid liner wall due to a temperature gradient within the wall and is defined as:

$$K_{1-2} = \frac{k_w}{t_w}(T_{w1} - T_{w2}) \tag{3.34}$$

In the following section, expressions for Equation (3.32) are derived. When inserted into Equation (3.32), they allow liner-wall temperatures to be calculated for any combustor inlet conditions of pressure, temperature, air mass flow rate and air/fuel ratio.

Internal Radiation

In most gas turbine combustors a sizeable portion of the heat transferred from the hot gases contained within the liner wall is by thermal radiation. Thermal radiation has two components:

- Nonluminous radiation (CO_2, H_2O vapor)
- Luminous radiation (mainly soot)

Both modes of radiant heat transfer enter into the calculations of the liner wall temperature and the amount of air to be employed in liner-wall cooling.

Radiation from Nonluminous Gases

The net radiant heat transfer is given by

$$R_1 = \sigma(\varepsilon_g T_g^4 - \alpha_g T_{w1}^4) \tag{3.35}$$

Gas emissivity ε_g depends on T_g, and gas absorptivity α_g on T_{w1}. In practice the surface exposed to the flame is not black, but has an effective absorptivity that is less than unity. According to Lefebvre, for most practical purposes this effect may be accounted for by introducing the factor $0.5(1+\varepsilon_w)$ to obtain

$$R_1 = 0.5\sigma(1+\varepsilon_w)(\varepsilon_g T_g^4 - \alpha_g T_{w1}^4) \tag{3.36}$$

The wall emissivity ε_w depends on the wall material and temperature. Approximate mean values of ε_w at typical liner-wall temperatures for Nimonic and stainless steel are 0.7 and 0.8.

Investigations over a wide range of values by Lefebvre show that a sufficient approximation is:

$$\frac{\alpha_g}{\varepsilon_g} = \left(\frac{T_g}{T_{w1}}\right)^{1.5} \tag{3.37}$$

Hence, Equation (3.36) may be rewritten as:

$$R_1 = 0.5\sigma(1+\varepsilon_w)\,\varepsilon_g T_g^{1.5}(T_g^{2.5} - T_{w1}^{2.5}) \tag{3.38}$$

Values of ε_g for nonluminous flames may be obtained from the following approximate formula (Lefebvre. 1999):

$$\varepsilon_g = 1 - \exp\left[-290P(\mathrm{FA}\, l_b)^{0.5} T_g^{-1.5}\right] \tag{3.39}$$

The mean beam length l_b is determined by the size and shape of the gas volume. For most practical purposes a sufficient expression is:

$$l_b = 3.4 \frac{\text{Volume}}{\text{Surface Area}} \tag{3.40}$$

For tubular systems the above expression yields values of mean beam length ranging from $0.6D_L$ to $0.9D_L$, depending on the length/diameter ratio of the liner. For annular combustors, l_b is $1.0D_L$ for the inner liner and $1.2D_L$ for the outer liner (Lefebvre. 1999).

Radiation from Luminous Gases

At high levels of pressure, soot particles can attain sufficient size and concentration to radiate as blackbodies. According to Lefebvre, the influence of luminosity on gas emissivity may be accounted for by including a luminosity factor L into Equation (3.39)

$$\varepsilon_g = 1 - \exp\left[-290PL(\mathrm{q}\, l_b)^{0.5} T_g^{-1.5}\right] \tag{3.41}$$

The original equation for L by Lefebvre was:

$$L = 7.53(C/H - 5.5)^{0.84} \tag{3.42}$$

C/H is the carbon/hydrogen ratio of the fuel by mass. Lefebvre has later correlated modern engine combustor data using:

$$L = 336/H^2 \tag{3.43}$$

H is the fuel hydrogen content (by mass) in percent.

For any given fuel type, the luminosity factor L may be calculated from one of these equations and inserted in to Equation (3.41) to obtain the luminous flame emissivity ε_g. Substituting this value of ε_g into Equation (3.38) gives the radiation heat flux from the flame to the liner wall.

External Radiation

The amount of radiant heat transferred from the liner to the outside casing is typically quit small compared with C_2, the external convective heat transfer rate. Its significance increases with liner wall temperature, and at low values it can often be neglected. It can be estimated only approximately because of a lack of accurate knowledge of wall emissivities. For this reason, it is sufficient to use the cooling-air temperature T_3 in place of the unknown temperature of the outer casing. For radiation across a long annular space, the geometric shape factor is assumed equal to unity. That gives us the following expression for the net radiation (Lefebvre. 1999):

$$R_2 = \sigma \frac{\varepsilon_w \varepsilon_g}{\varepsilon_c + \varepsilon_w (1-\varepsilon_c)(A_w / A_c)} \left(T_{w2}^4 - T_3^4\right) \tag{3.44}$$

For a tubular chamber, A_w / A_c is equal to the ratio of liner diameter to casing diameter. For tuboannular systems, in which the depth of annulus varies from point to point around the liner, an average value of 0.8 should be used. For an annular chamber, the ratio A_w / A_c is slightly greater than unity for the inner liner, and slightly less than unity for the outer liner.

According to Lefebvre (1999), for most practical purposes, the following expressions, based on typical values of emissivity and diameter ratio, are sufficient.

For an aluminum air casing:

$$R_2 = 0.4\sigma (T_{w2}^4 - T_3^4) \tag{3.45}$$

For a steel air casing:

$$R_2 = 0.6\sigma (T_{w2}^4 - T_3^4) \tag{3.46}$$

Internal Convection

Of the four heat-transfer processes that together determine the liner temperature, internal convection is the most difficult to estimate accurately. In the primary zone the gases involved in heat transfer are at high temperature and are undergoing rapid physical and chemical changes. Further difficulty is introduced by the existence within the primary zone of steep gradients of temperature, velocity, and composition. Uncertainties regarding the airflow pattern, the state of boundary-layer development, and the effective gas temperature make the choice of a realistic model almost arbitrary.

In the absence of more exact data, it is reasonable to assume that some form of the classical heat-transfer relation for straight pipes will hold for conditions inside a liner, provided the Reynolds number index is consistent with established practice for conditions of extreme turbulence. This leads to an expression of the form (Lefebvre. 1999)

$$C_1 = 0.020 \frac{k_g}{D_L^{0.2}} \left(\frac{\dot{m}_g}{A_L \, \mu_g} \right)^{0.8} \left(T_g - T_{w1} \right) \tag{3.47}$$

Where D_L is the hydraulic diameter of the liner:

$$D_L = 4 \frac{\text{cross-sectional flow area}}{\text{wetted perimeter}} \tag{3.48}$$

The gas temperature T_g is appropriate for radiation, but the conventional primary-zone radial temperature profile is deliberately arranged to provide lower-than-average gas temperatures near the wall. To account for this, the value of the constant in Equation (3.47) is reduced from 0.020 to 0.017 so that, for calculations in the primary zone, Equation (3.47) becomes (Lefebvre. 1999):

$$C_{1,pz} = 0.017 \frac{k_g}{D_L^{0.2}} \left(\frac{\dot{m}_{pz}}{A_L \, \mu_g} \right)^{0.8} \left(T_g - T_{w1} \right) \tag{3.49}$$

External Convection

Similar to internal convection, the Reynolds number is now based on the hydraulic mean diameter D_{an} of the annulus air space. This diameter is given by

$$D_{an} = 4\frac{\text{cross-sectional area of flow}}{\text{wetted perimeter}} \tag{3.50}$$

Diameter of an annulus air space for a tubular chamber:

$$D_{an} = D_{ref} - D_L \tag{3.51}$$

Diameter of an annulus air space for a annular chamber:

$$D_{an} = 2 \text{ x local annulus height} \tag{3.52}$$

The contents of the annulus may be assumed sufficiently stirred for fully developed turbulent transfer to occur. The external convection is now:

$$C_2 = 0.020\frac{k_a}{D_{an}^{0.2}}\left(\frac{\dot{m}_{an}}{A_{an}\,\mu_a}\right)^{0.8}\left(T_{w2} - T_3\right) \tag{3.53}$$

The fluid properties are now evaluated at the annulus air temperature T_3. In practice the cooling-air temperature will increase during the passage downstream.

Heat transfer Resistance Model

The heat transfer resistance model is applied to find the heat transfer coefficient *h* used in Equation(3.8). The assumption for a thin liner wall of Equation(3.33) applies here as well, therefore Equation(3.8) can be written as:

$$q = h\left(T_g - T_a\right) \tag{3.54}$$

The coefficient *h* includes internal radiation (R_1) and convection (C_1), conduction $K_{1\text{-}2}$ plus external radiation (R_2) and convection (C_2). To find *h*, the thermal circuit model shown in Figure 3-7 is used. The resistance *R* is defined by:

$$R = \frac{1}{h} \tag{3.55}$$

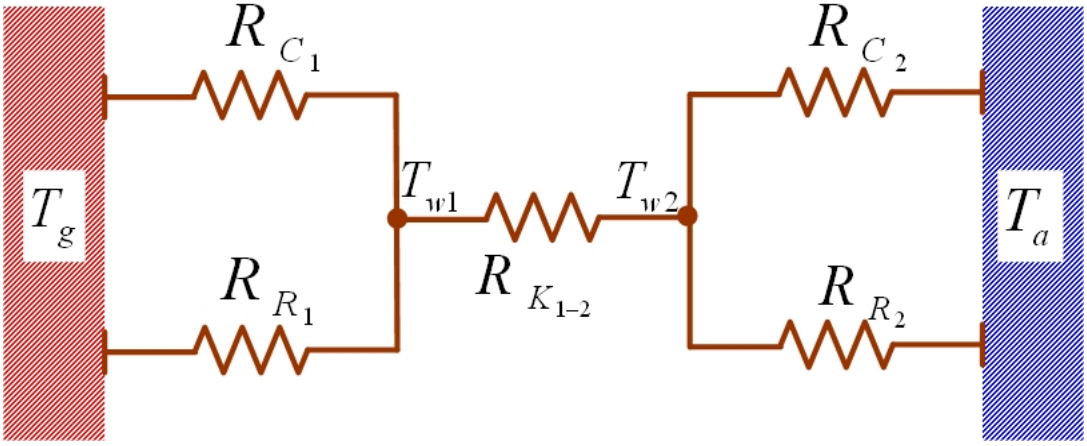

Figure 3-7 Thermal circuit of the combustor

The heat transfer from internal convection (C_1) can be expressed as:

$$C_1 = h_{C_1}\left(T_g - T_{w1}\right) \tag{3.56}$$

Knowing Equation (3.47), h_{C_1} can be defined as:

$$h_{C_1} = 0.020\frac{k_g}{d_L^{0.2}}\left(\frac{\dot{m}_g}{A_L\,\mu_g}\right)^{0.8} \tag{3.57}$$

By the Equation (3.53), the coefficient h_{C_2} for external convection is:

$$h_{C_2} = 0.020\frac{k_a}{D_{an}^{0.2}}\left(\frac{\dot{m}_{an}}{A_{an}\,\mu_a}\right)^{0.8} \tag{3.58}$$

To find the heat transfer coefficient (h_{R1}) for the internal radiation (R_1), a gas temperature dependent coefficient is applied to bring the $(T_g - T_{w1})$ term into Equation(3.38).

$$h_{R_1} = 0.5\sigma\left(1+\varepsilon_w\right)\varepsilon_g\left(T_g^2 + T_{w1}^2\right)\left(T_g + y_{lin}\,T_{w1}\right) \tag{3.59}$$

The coefficient y_{lin} was found empirical over by several iterations for T_g values, where the original Equation (3.38) for internal radiation was compared to the modified expression with the new coefficient.

$$y_{lin} = -8.919454\cdot10^{-8}\,T_g^2 + 3970659\cdot10^{-4}\,T_g - 1.772502\cdot10^{-3} \tag{3.60}$$

The external radiation coefficient (h_{R2}) is given by rewriting the temperature term of Equation(3.44).

$$h_{R_2} = \sigma \frac{\varepsilon_w \varepsilon_g}{\varepsilon_c + \varepsilon_w (1-\varepsilon_c)(A_w / A_c)} \left(T_{w2}^2 + T_a^2\right)\left(T_{w2} + T_a\right) \tag{3.61}$$

The conduction *h* coefficient is found by Equation(3.34):

$$h_{K_{1-2}} = \frac{k_w}{t_w} \tag{3.62}$$

As shown in Figure 3-7, the internal convection and radiation resistances are parallel. The overall resistance is given by:

$$R_{12} = \left[\frac{1}{R_{C_1}} + \frac{1}{R_{R_1}}\right]^{-1} \tag{3.63}$$

The total resistance for external convection and radiation is also parallel.

$$R_{45} = \left[\frac{1}{R_{C_2}} + \frac{1}{R_{R_2}}\right]^{-1} \tag{3.64}$$

The total resistance is the summation of the three resistances and can be substituted into Equation(3.55) to get the overall *h* coefficient, the one used in the energy balance.

$$h = \frac{1}{R_{12} + R_{K_{1-2}} + R_{45}} \tag{3.65}$$

Summary Mathematical Model

A summery of the key equations used in the developed mathematical model is shown by Table 3.1 - Table 3.5.

Table 3.1 Chemical species equations

(2.4)	$\phi = \frac{FA_{act}}{FA_{stoich}}$
(3.19)	$a_{CH_4}CH_4 + a_{O_2}O_2 + a_{N_2}N_2 + a_{H_2O}H_2O + a_{CO_2}CO_2 \longrightarrow b_{CO_2}CO_2 + b_{H_2O}H_2O + b_{O_2}O_2 + b_{N_2}N_2 + b_{CH_4}CH_4$
(3.20)	$a_{CH_4} = 1$
(3.21)	$a_{O_2} = \frac{f_{stoich}}{\phi}$
(3.22)	$a_{N_2} = \frac{f_{stoich}\,3.76}{\phi}$
(3.23)	$a_{H_2O} = a_{O_2}1.608\frac{0.622\,P_{sat}\,RH}{P_{atm}}$
(3.24)	$b_{CO_2} = a_{CH_4} + a_{CO_2}$
(3.25)	$b_{H_2O} = a_{H_2O} + f_{stoich}$
(3.26)	$b_{N_2} = a_{N_2}$
(3.27)	$b_{O_2} = a_{O_2} - f_{stoich}$
(3.28)	$\overline{c}_{p,ex} = \frac{b_{CO_2}\,\overline{c}_{p,CO_2} + b_{H_2O}\,\overline{c}_{p,H_2O} + b_{N_2}\,\overline{c}_{p,N2} + b_{O_2}\,\overline{c}_{p,O2}}{b_{CO_2} + b_{H_2O} + b_{N_2} + b_{O_2}}$

Table 3.2 Combustor inlet equations

(3.3)	$T_{2,s} = T_{amb}\left(PR\right)^{\frac{\gamma-1}{\gamma}}$
(3.4)	$T_2 = \frac{T_{2,s} - T_{amb}}{\eta_{s,comp}} + T_{amb}$
(3.5)	$w_{Comp} = \frac{c_{p,a\,T_{amb}} + c_{p,a\,T_2}}{2}\left(T_{amb} - T_2\right)$
(3.29)	$c_{p,ex} = \frac{\dot{m}_A\, c_{p,air\,A} + \dot{m}_B\, c_{p,ex\,B} + \dot{m}_C\, c_{p,ex\,C} + \dot{m}_D\, c_{p,air\,D}}{\dot{m}_A + \dot{m}_B + \dot{m}_C + \dot{m}_D}$
(3.30)	$w_{Comp} = w_{GPT}$
(3.31)	$T_{GPT} = T_{ex} - \frac{w_{GPT}}{c_{p,ex}}$

Table 3.3 Energy balance for a combustion zone, simultaneously solved

(3.13)	$\dot{E}_{A,in} = T_{ABC,in} c_{p,a} \dot{m}_A$
(3.14)	$\dot{E}_{A,out} = T_{ABC,out} c_{p,a} \dot{m}_A$
(3.15)	$\dot{E}_{B,in} = T_{ABC,in}\left[Zr_{B,i}\left(c_{p,a}\dot{m}_{B,a} + c_{p,f}\dot{m}_{B,f}\right) + Zp_{B,i}\, c_{p,ex\,pilot}\dot{m}_B \right] + Zr_{B,i}\, LHV\, \dot{m}_{B,f}$
(3.16)	$\dot{E}_{B,out} = T_{ABC,out}\left[Zr_{B,i+1}\left(c_{p,a}\dot{m}_{B,a} + c_{p,f}\dot{m}_{B,f}\right) + Zp_{B,i+1}\, c_{p,ex\,pilot}\dot{m}_B \right] + Zr_{B,i+1}\, LHV\, \dot{m}_{B,f}$
(3.17)	$\dot{E}_{C,in} = T_{ABC,in}\left[Zr_{C,i}\left(c_{p,a}\dot{m}_{C,a} + c_{p,f}\dot{m}_{C,f}\right) + Zp_{C,i}\, c_{p,ex\,main}\dot{m}_C \right] + Zr_{C,i}\, LHV\, \dot{m}_{C,f}$
(3.18)	$\dot{E}_{C,out} = T_{ABC,out}\left[Zr_{C,i+1}\left(c_{p,a}\dot{m}_{C,a} + c_{p,f}\dot{m}_{C,f}\right) + Zp_{C,i+1}\, c_{p,ex\,main}\dot{m}_C \right] + Zr_{C,i+1}\, LHV\, \dot{m}_{C,f}$
(3.6)	$\dot{E}_{D,in} = T_{D,in}\, c_{p,a}\, \dot{m}_D$
(3.9)	$\dot{E}_{D,out} = T_{D,out}\, c_{p,a}\, \dot{m}_D$
(3.7)	$\dot{E}_{ABC,in} = \dot{E}_{A,in} + \dot{E}_{B,in} + \dot{E}_{C,in}$
(3.11)	$\dot{E}_{ABC,out} = \dot{E}_{A,out} + \dot{E}_{B,out} + \dot{E}_{C,out}$
(3.10)	$\dot{E}_{D,in} + \dot{Q} = \dot{E}_{D,out}$
(3.12)	$\dot{E}_{ABC,in} - \dot{Q} = \dot{E}_{ABC,out}$
(3.8)	$\dot{Q} = h\,A(T_{ABC,out} - T_{D,out})$

Table 3.4 Heat transfer equations, simultaneously solved

(3.34)	$K_{1-2} = \frac{k_w}{t_w}(T_{w1} - T_{w2})$
(3.38)	$R_1 = 0.5\sigma(1+\varepsilon_w)\,\varepsilon_g T_g^{1.5}(T_g^{2.5} - T_{w1}^{2.5})$
(3.49)	$C_{1,pz} = 0.017\frac{k_g}{D_L^{0.2}}\left(\frac{\dot{m}_{pz}}{A_L\,\mu_g}\right)^{0.8}\left(T_g - T_{w1}\right)$
(3.44)	$R_2 = \sigma\frac{\varepsilon_w\,\varepsilon_g}{\varepsilon_c + \varepsilon_w(1-\varepsilon_c)(A_w/A_c)}\left(T_{w2}^4 - T_3^4\right)$
(3.53)	$C_2 = 0.020\frac{k_a}{D_{an}^{0.2}}\left(\frac{\dot{m}_{an}}{A_{an}\,\mu_a}\right)^{0.8}\left(T_{w2} - T_3\right)$
(3.32)	$R_1 + C_1 = K_{1-2}$
(3.32)	$R_2 + C_2 = K_{1-2}$

Table 3.5 Heat transfer resistance model equations

(3.57)	$h_{C_1} = 0.020\frac{k_g}{d_L^{0.2}}\left(\frac{\dot{m}_g}{A_L\,\mu_g}\right)^{0.8}$
(3.58)	$h_{C_2} = 0.020\frac{k_a}{D_{an}^{0.2}}\left(\frac{\dot{m}_{an}}{A_{an}\,\mu_a}\right)^{0.8}$
(3.59)	$h_{R_1} = 0.5\,\sigma(1+\varepsilon_w)\,\varepsilon_g\left(T_g^2 + T_{w1}^2\right)\left(T_g + y_{lin}\,T_{w1}\right)$
(3.61)	$h_{R_2} = \sigma\frac{\varepsilon_w\,\varepsilon_g}{\varepsilon_c + \varepsilon_w(1-\varepsilon_c)(A_w/A_c)}\left(T_{w2}^2 + T_a^2\right)\left(T_{w2} + T_a\right)$
(3.62)	$h_{K_{1-2}} = \frac{k_w}{t_w}$
(3.55)	$R_i = \frac{1}{h_i}$
(3.63)	$R_{12} = \left[\frac{1}{R_{C_1}} + \frac{1}{R_{R_1}}\right]^{-1}$
(3.64)	$R_{45} = \left[\frac{1}{R_{C_2}} + \frac{1}{R_{R_2}}\right]^{-1}$
(3.65)	$h = \frac{1}{R_{12} + R_{K_{1-2}} + R_{45}}$

CHAPTER 4 - Model Development

The previous derived equations were modeled using a FORTRAN program called "Kombust." The program is based on a SOLAR Taurus 70 gas turbine. More information about the SOLAR gas turbine can be found in Chapter 5.

Figure 4-1 shows the flow diagram of the developed "Kombust" FORTRAN program. Inputs to the program are conditions such as ambient temperature and pressure, relative humidity and load applied to the gas turbine. Turbine specific inputs such as geometry and efficiencies are directly defined inside the FORTRAN code. Because of a confidentiality agreement between SOLAR and the NGML, these data are not accessible by the user. Based on the applied load, Kombust first calculates the discharger pressure, air and fuel flows. These data are found by applying linear functions through a turbine data file. By knowing the fuel and air flows at a specific turbine load, Kombust calculates the equivalence ratio and the exact amount of the chemical species in the fuel/air mixture. With the given discharge pressure and an assumed compressor efficiency, the combustor inlet temperature can also be calculated.

After knowing the inlet conditions, a combustion routine calculates the different zone temperatures using the Newton-Raphson method for applying the energy balance and heat transfer equations. With the zone temperatures can then the formation of NO_x and CO be predicted using several correlations by various researchers described in chapter 2. At the end, all the calculated values are written into an output file, which is accessible for the user.

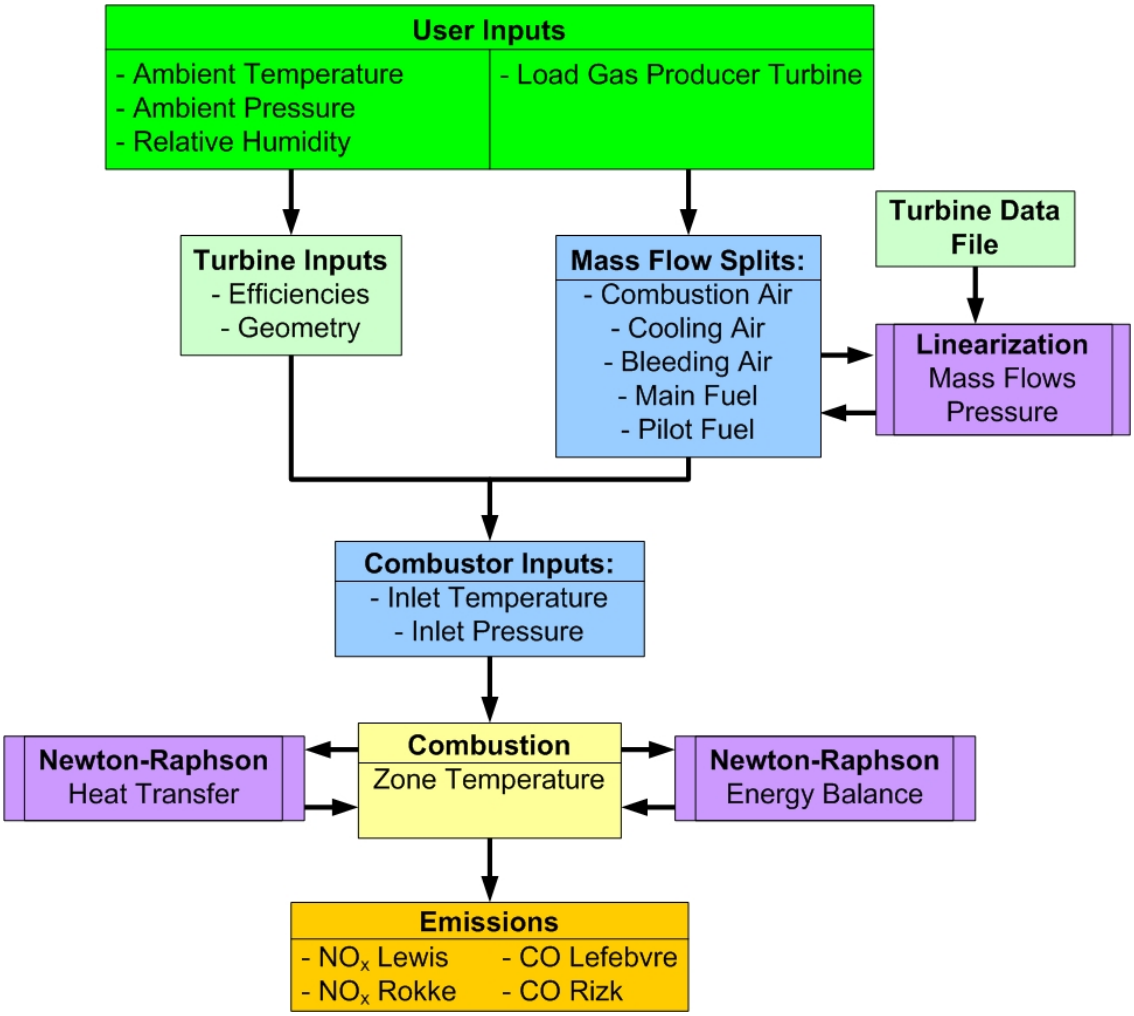

Figure 4-1 Flow diagram Kombust program

The three purple colored boxes in the previous flow chart, each box with the two vertical lines inside, are IMSL functions. IMSL stands for International Mathematical and Statistical Library. The Kombust model embeds two algorithms from these libraries, called last squares method and Newton-Raphson method.

Least Squares Method

To find a linear function for mass flow or fuel flow, the least squares method given by the IMSL functions was applied. A linear function is expressed by (Ott, et al. 2004):

$$y = \hat{\alpha} + \hat{\beta}x \tag{4.1}$$

Assuming that there is given a set of x and y values where the linear function needs to be found. First sum the x and y observations, the squares of x's and the products of xy to obtain the following quantities:

$$S_x = x_1 + x_2 + ... + x_n \tag{4.2}$$

$$S_y = y_1 + y_2 + ... + y_n \tag{4.3}$$

$$S_{xx} = x_1^2 + x_2^2 + ... + x_n^2 \tag{4.4}$$

$$S_{xy} = x_1 y_1 + x_2 y_2 + ... + x_n y_n \tag{4.5}$$

The summary statistics from Equation(4.2) to (4.5) is used to solve for $\hat{\beta}$.

$$\hat{\beta} = \frac{nS_{xy} - S_x S_y}{nS_{xx} - S_x S_x} \tag{4.6}$$

Now knowing $\hat{\beta}$, $\hat{\alpha}$ is found by:

$$\hat{\alpha} = \frac{S_y - \hat{\beta} S_x}{n} \tag{4.7}$$

The estimated line will always pass through the center. The least square estimation for linear models is notoriously non-robust to outliers (Ott, et al. 2004).

Newton-Raphson Method

To find the values of n-unknowns in a set of n-equations, a method called Newton-Raphson from the IMSL library is applied. Figure 4-2 shows an illustration of one iteration of Newton-Raphson's method. The concept of the method is as follows: One starts with an initial guess that is reasonably close to the true root. Then the function is approximated by its tangent line (which can be computed using the tools of calculus), and one computes the x-axis intercept will typically be a better approximation to the functions root than the original guess, and the method can be iterated. It can be seen that the second trial (x_{n+1}) is a better approximation than the first trial (x_n) for the root x of the function *f*.

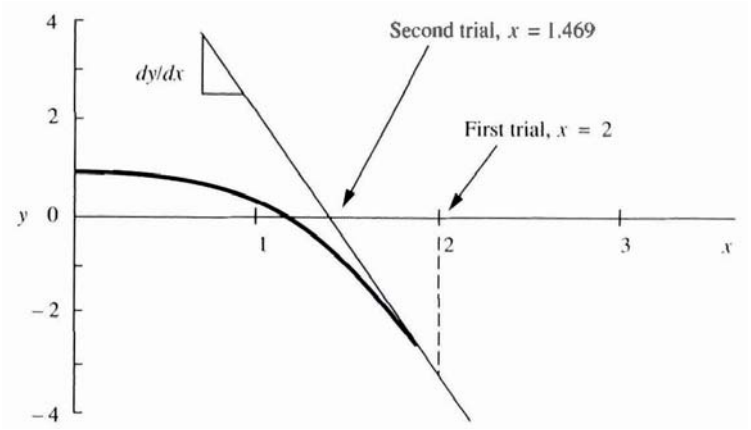

Figure 4-2 Newton-Raphson iteration
Source (Stoecker. 1989)

As described by Stoecker (1989), the procedure for solving the equations is iterative in which the following steps are followed, supposed that three nonlinear equations are be solved for the three unknown variables x_1,x_2 and x_3:

$$f_1(x_1, x_2, x_3) = 0 \tag{4.8}$$

$$f_2(x_1, x_2, x_3) = 0 \tag{4.9}$$

$$f_3(x_1, x_2, x_3) = 0 \tag{4.10}$$

1. Rewrite the equations so that all terms are on one side of the equality sign (Equation(4.8) - (4.10) already exist in this from)
2. Assume temporary values for the variables, denote $x_{1,t}, x_{2,t}$, and $x_{3,t}$

3. Calculate the values of f_1, f_2 and f_3 at the temporary values of x_1, x_2, and x_3
4. Compute the partial derivatives of all functions with respect to all variables.
5. Use the Taylor-series expansion of the form of Equation(4.11) to establish a set of simultaneous equations.

$$\begin{aligned} y(x_1, x_2, ..., x_3) \quad = \quad & y(a_1, a_2, ..., a_n) \\ & + \sum_{j=1}^{n} \frac{\partial y(a_1, ..., a_n)}{\partial x_j}(x_j - a_j) \\ & + \frac{1}{2}\sum_{i=1}^{n}\sum_{j=1}^{n} \frac{\partial^2 y(a_1, ..., a_n)}{\partial x_i \partial x_j}(x_i - a_i)(x_j - a_j) + ... \end{aligned} \tag{4.11}$$

The Taylor-series expansion for Equation(4.8), for example, is

$$\begin{aligned} f_1(x_{1,t}, x_{2,t}, x_{3,t}) \quad \approx \quad & f_1(x_{1,c}, x_{2,c}, x_{3,c}) \\ & + \frac{\partial f_1(x_{1,t}, x_{2,t}, x_{3,t})}{\partial x_1}(x_{1,t} - x_{1,c}) \\ & + \frac{\partial f_1(x_{1,t}, x_{2,t}, x_{3,t})}{\partial x_2}(x_{2,t} - x_{2,c}) \\ & + \frac{\partial f_1(x_{1,t}, x_{2,t}, x_{3,t})}{\partial x_3}(x_{3,t} - x_{3,c}) \end{aligned} \tag{4.12}$$

The set of equations is

$$\begin{bmatrix} \frac{\partial f_1}{\partial x_1} & \frac{\partial f_1}{\partial x_2} & \frac{\partial f_1}{\partial x_3} \\ \frac{\partial f_2}{\partial x_1} & \frac{\partial f_2}{\partial x_2} & \frac{\partial f_2}{\partial x_3} \\ \frac{\partial f_3}{\partial x_1} & \frac{\partial f_3}{\partial x_2} & \frac{\partial f_3}{\partial x_3} \end{bmatrix} \begin{bmatrix} x_{1,t} - x_{1,c} \\ x_{2,t} - x_{2,c} \\ x_{3,t} - x_{3,c} \end{bmatrix} = \begin{bmatrix} f_1 \\ f_2 \\ f_3 \end{bmatrix} \tag{4.13}$$

6. Solve the set of linear simultaneous Equations(4.13) to determine $x_{i,t} - x_{i,c}$
7. Correct the *x*'s

$$\begin{aligned} x_{1,\text{new}} &= x_{1,\text{old}} - (x_{1,t} - x_{1,c}) \\ x_{2,\text{new}} &= x_{2,\text{old}} - (x_{2,t} - x_{2,c}) \\ x_{3,\text{new}} &= x_{3,\text{old}} - (x_{3,t} - x_{3,c}) \end{aligned} \tag{4.14}$$

8. Test for convergence. If the absolute magnitudes of all the *f*'s or all the Δx's are satisfactorily small, terminate; otherwise return to step 3.

Cp Functions

The Kombust model has implemented c_p correlations for all the products and reactants assuming a complete combustion process between a lean mixture of methane and air. The c_p value of any gas can be called at any point of the program knowing the temperature.

Figure 4-3 shows a graph of the c_p functions between a temperature range of 400-2000 Kelvin. A methane/air mixture with 50 percent excess air was used to calculate the c_p exhaust. From the previous equilibrium example in chapter 2, it is known that around 73 percent of the exhaust in this mixture is nitrogen. Hence, it is not surprising that c_p exhaust has the trend of c_p nitrogen. The c_p value of the exhaust is a little bit higher since 13 percent of the exhaust is water vapor, which has a higher amount of energy compared to nitrogen at the same temperature.

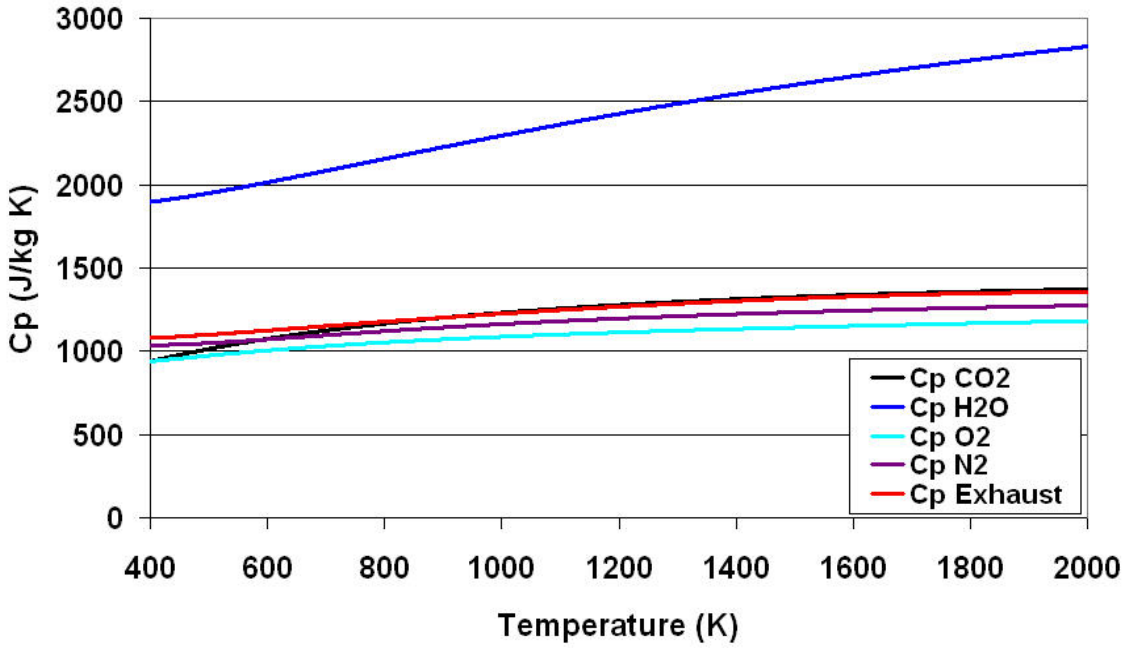

Figure 4-3 c_p values as function of temperature

The c_p correlation for air used in the Kombust model is given by Cengel (Cengel, Y.A. Boles, M.A. 2002). The average error between a temperature range of 273-1800 Kelvin is 0.33 percent.

$$c_{p,\mathrm{Air}} = \left(28.11 + 0.1967 \cdot 10^{-2} T + 0.4802 \cdot 10^{-5} T^2 - 1.966 \cdot 10^{-9} T^3\right) \cdot \frac{10^3}{M_{\mathrm{Air}}} \qquad (4.15)$$

For N_2, CO_2, H_2O, O_2 and CH_4, reactants and products of a complete combustion process, c_p correlations proposed by Sonntag (Sonntag, et al. 1998) are used. These correlations have a maximal error of 0.43 percent within a temperature range of 300-2000 Kelvin.

$$c_{p,\mathrm{N_2}} = \left(39.06 - 512.79\left(\frac{T}{100}\right)^{-1.5} + 1072.7\left(\frac{T}{100}\right)^{-2} - 820.4\left(\frac{T}{100}\right)^{-3}\right) \cdot \frac{10^3}{M_{\mathrm{N_2}}} \qquad (4.16)$$

$$c_{p,\mathrm{CO_2}} = \left(-3.7357 + 30.529\left(\frac{T}{100}\right)^{0.5} - 4.103\left(\frac{T}{100}\right) + 0.024196\left(\frac{T}{100}\right)^{2}\right) \cdot \frac{10^3}{M_{\mathrm{CO_2}}} \qquad (4.17)$$

$$c_{p,\mathrm{H_2O}} = \left(143.05 - 183.54\left(\frac{T}{100}\right)^{0.25} + 82.751\left(\frac{T}{100}\right)^{0.5} - 3.6989\left(\frac{T}{100}\right)\right) \cdot \frac{10^3}{M_{\mathrm{H_2O}}} \qquad (4.18)$$

$$c_{p,\mathrm{O_2}} = \left(37.432 + 0.020102\left(\frac{T}{100}\right)^{1.5} - 178.57\left(\frac{T}{100}\right)^{-1.5} + 236.88\left(\frac{T}{100}\right)^{-2}\right) \cdot \frac{10^3}{M_{\mathrm{O_2}}} \qquad (4.19)$$

$$c_{p,\mathrm{CH_4}} = \left(-672.87 + 439.74\left(\frac{T}{100}\right)^{0.25} - 24.875\left(\frac{T}{100}\right)^{0.75} + 323.88\left(\frac{T}{100}\right)^{-0.5}\right) \cdot \frac{10^3}{M_{\mathrm{CH_4}}} \qquad (4.20)$$

CHAPTER 5 - Validation

To validate the Kombust model to a real gas turbine, a data set from a SOLAR Taurus 70 low emission gas turbine was used. The first section of this chapter explains some basic information about the unit and then shows the operating and emissions trends of the given data.

SOLAR Taurus 70

The validation was done on a SOLAR Taurus 70 gas turbine unit. Figure 5-1 shows the gas turbine mechanical-drive package for the oil and gas industry. The unit is approximately 7.3 meter long, has a width of 2.7 meter and a height of 3.6 meter. It is a two shaft industrial turbine. It has a 14 stage axial compressor with variable inlet guide vanes. The target compressor and gas producer turbine speed of is 15,200 rpm. At half load, the gas producer speed decreases down to a approximately 14,000 rpm or 92 percent of the target speed.

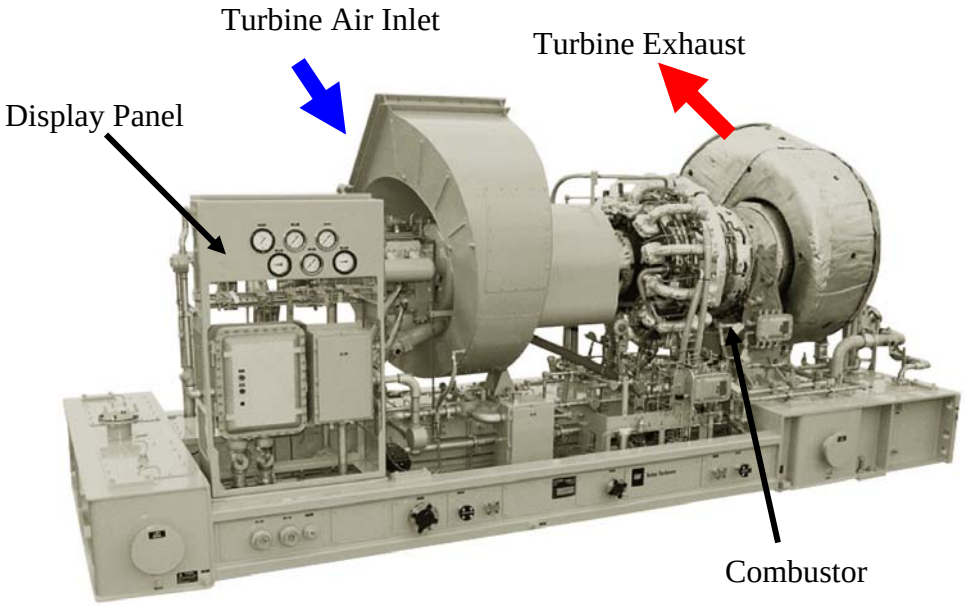

Figure 5-1 SOLAR Taurus 70 gas turbine unit

Source: SOLAR web page (http://mysolar.cat.com)

The turbine produces under normal rated ISO conditions (15°C, sea level) 7,690kW (10,310hp). Figure 5-2 shows a graph of the inlet air temperature versus output power. The figure shows that changes in ambient temperature have an impact on full-load power and heat rate. The higher the ambient temperature, the lower the power output and the higher the heat rate. The same effect can be seen at part-load performance.

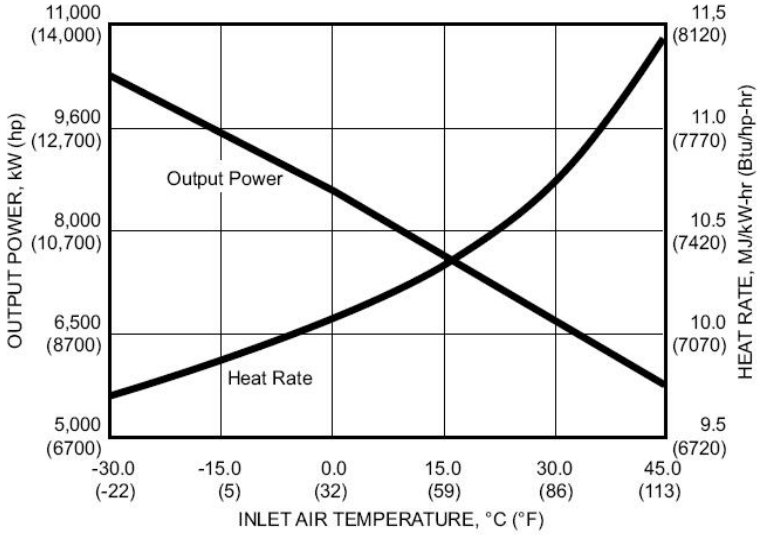

Figure 5-2 Available power SOLAR Taurus 70

Source: Solar web page (http://mysolar.cat.com)

The ambient pressure also impacts power output. The air density reduces at lower ambient pressures, due to elevation or changing atmospheric conditions. Lower density means lower air mass flow while the actual volumetric flow is unchanged. The density affects only the power output but not the efficiency of the engine. The impact of the relative humidity on engine performance for low ambient temperatures is negligible, since the water concentration in the air is low. At high ambient temperature, a high water content can cause a variety of changes in the engine. Some engine performance increases while other engine performance reduces (Kurz, et al. 2003). Any gas turbine will experience a reduced efficiency at part load. According to SOLAR, the engine efficiency of the Taurus 70 is 35.7% at standard conditions and full load. A more detailed description of the SOLAR Taurus 70 is in Appendix A.

SoLoNOx Control System Description

The gas turbine unit used for the data validation has a SoLoNOx combustor. This combustor works like the dry lean concept which was explained in Chapter 2. The cross-section of the SoLoNOx combustion system is shown in Figure 5-3. To broaden the low emissions operating range, SoLoNOx gas turbines use combustor air flow control within the gas turbine to maintain an approximately constant primary zone flame temperature. The primary zone is the part of the combustor directly downstream of the fuel injector where peak combustion temperatures and the highest NO_x formation rates occur. Combustor air flow control is achieved by controlling the compressor air bleed at part load for two-shaft engines. Figure 5-3 indicates the air flow patterns through the combustor and the bleed system to the exhaust. As bleed air is pulled from the combustor case the fuel/air ratio and corresponding primary zone flame temperature are maintained relatively constant as engine load is reduced. SoLoNOx engines operate with very low emissions signature to approximately 50% of full load power.

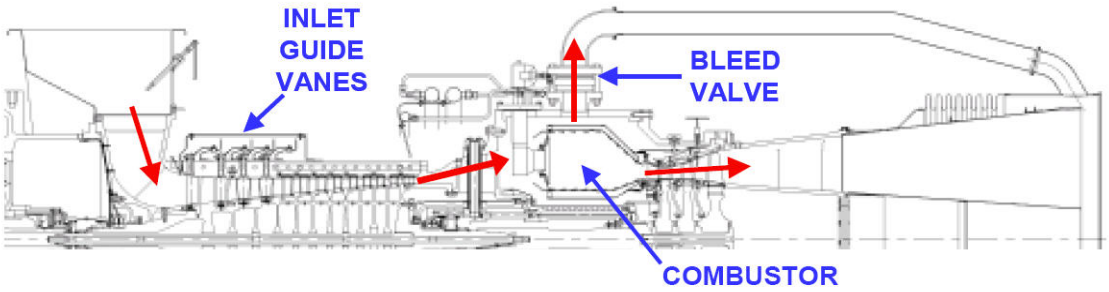

Figure 5-3 SoLoNOx air flow control through the combustor
Source: SOLAR

On two shaft engines power output is not measured so the gas producer turbine speed (NGPT) is used in the control algorithms to approximate power and trigger engine controls for low emissions. Since the primary zone flame temperature (T_{pz}) is not measured directly, it is necessary to use a measured temperature within the turbine section (T_5). The T_5 probes are located between the gas producer and power turbine. In practice T_5 varies proportionately with primary zone flame temperature, but it is not a

direct surrogate. The relationship between T_5, NGPT, and emissions is shown in Figure 5-4. The bleed air flow rate is controlled by regulating the extent to which the bleed valve is open. The bleed valve position is controlled based on keeping a constant T_5 set-point equal to the measured T_5. Bleed valve T_5 set-point values are determined in the factory during engine testing for each unit at multiple engine speed operating points to maintain emissions at acceptable levels. Typical T_5 set-point values are indicated in Figure 5-4.

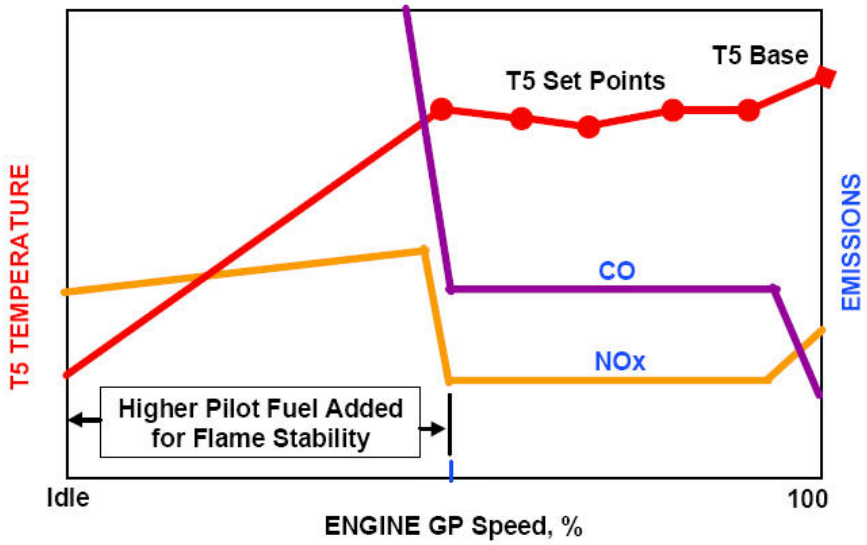

Figure 5-4 Comparison between a conventional and a lean-premixed combustor
Source: SOLAR

The other primary control parameter in the SoLoNOx gas turbine is the fuel split between main and pilot injection points. Main fuel is thoroughly premixed with combustion air prior to combustion and burns with a clean emissions signature. The balance of the fuel is delivered as pilot fuel that burns as a diffusion flame and provides flame stability. The different pilot control modes and their general influence on emissions are illustrated in Figure 5-5. During light-off and low-load operation, approximately 30 to 50% of the fuel passes through the pilot injector passages, providing a rich fuel/air mixture. Combustor stability is enhanced in this mode compared to lean-premixed operation, although NO_x and CO emissions are higher. Above 50% engine load, the pilot

fuel is reduced to a low amount of total fuel flow to optimize emissions performance. The pilot fuel is also increased during load transients to help stabilize the flame.

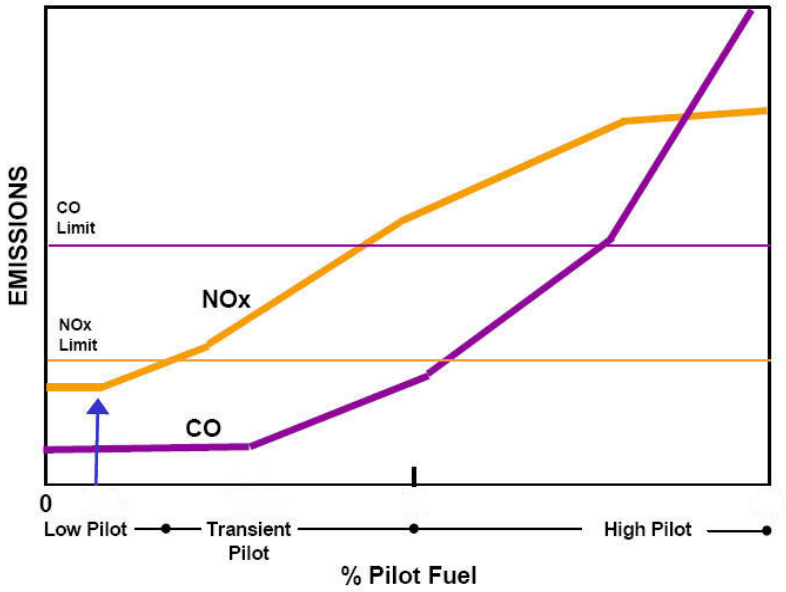

Figure 5-5 Influence of percent pilot fuel on emissions

Source: SOLAR

SOLAR Test Cell Data

The data was collected from two different engines on the test cell at SOLAR in San Diego, California. For each engine, two data points at full load and three data points at half load were recorded. The average ambient temperature for all ten points was 290 Kelvin, with an average relative humidity of 65%. No statistical information was provided by SOLAR regarding the accuracy of the data.

The collected data from the test cell are confidential and no emissions or other turbine values are published.

Mass Flows

The mass flow and compressor pressure data of this test set is used for the Kombust mass flow input file. Figure 5-6 shows the air flow at full load and half load. There is only a small variance between the data, with a strong trend to linearity seen by the R^2 factor which is almost equal to one. An R^2 value of one indicates that the fitted model explains all variability, an R^2 value of zero indicates no relationship between model and data. The line in the graph represents the linear trend line added to the data set.

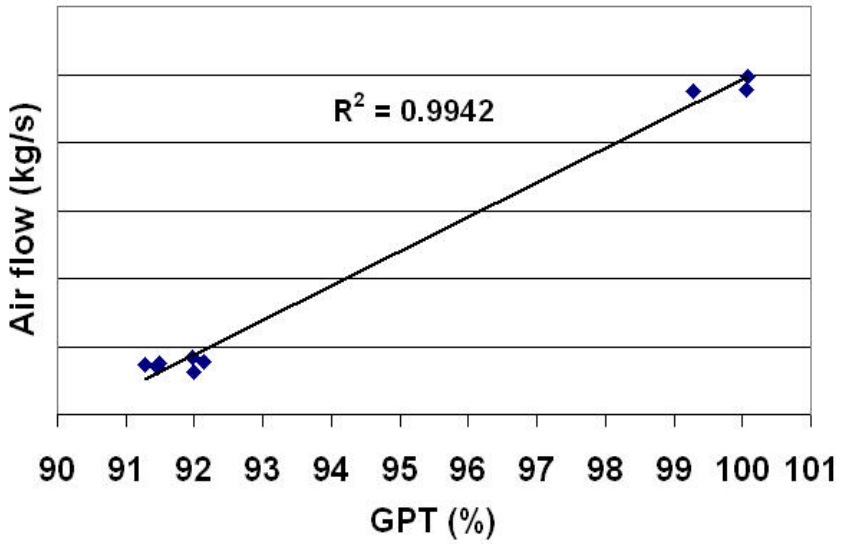

Figure 5-6 Gas producer turbine speed versus air flow

Graphs of the compressor pressure ratio, main fuel flow and bleed air from this data set are in Appendix B. All graphs have an R^2 value close to one. Unfortunately, these statements must be qualified by noting that the test cell data only has samples at full and half load and no data points in between these two loads. However, compressor flow rate is an approximate linear function of compressor speed (Boyce. 2002).

The only “inconsistent” data are from the pilot burner, shown in Figure 5-7. The difference between some data points at similar speed is up to 50 percent. The data show only a small trend to linearity with an R^2 value of 0.62. The gas turbine control system uses the pilot fuel to keep the measure temperature T_5 at a constant value. If the combustion temperature is two low or high, the amount of pilot fuel changes to achieve a certain temperature.

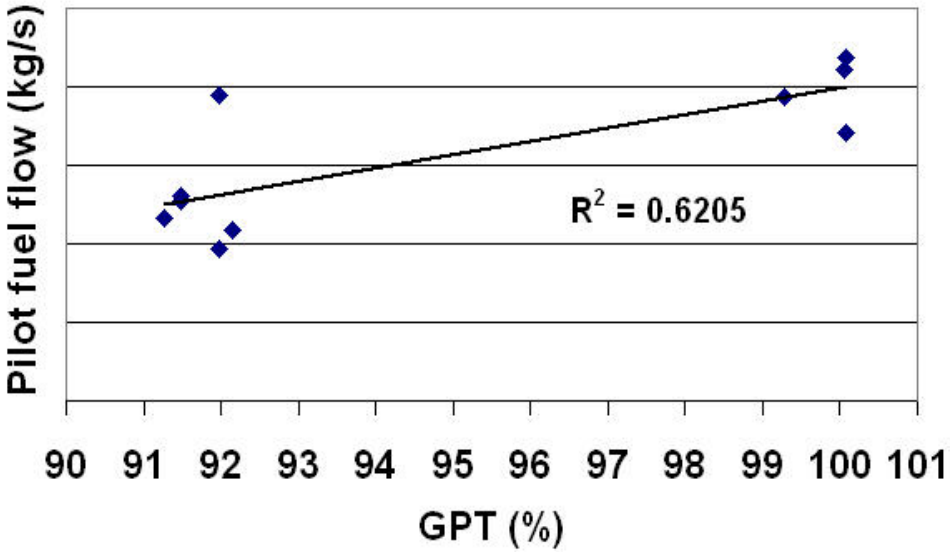

Figure 5-7 Gas producer turbine speed versus pilot fuel flow

Emissions

For each test cell data point, emission samples of NO_x and CO were recorded. Figure 5-8 shows NO_x versus gas producer speed, with a strong load dependency. At half load, the NO_x emissions were approximately 10 ppm lower than at full load. That suggests a lower combustion temperature at lower load because the NO_x formation is mainly a function of temperature. The two emissions points in red circles do not follow the trend of the others and may be in error.

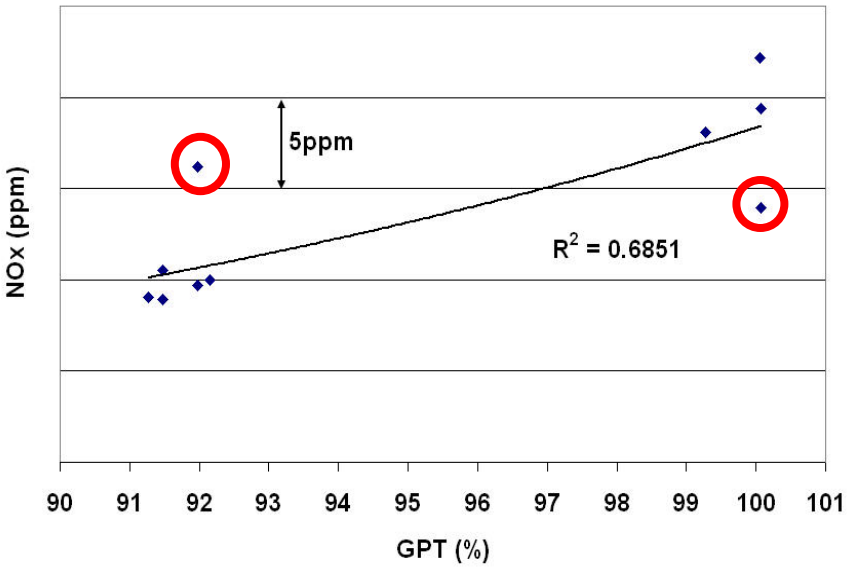

Figure 5-8 Gas producer turbine speed versus NO_x

To further determine the accuracy of these two data points, the emissions data were compared to each other. NO_x is plotted as a function of CO, shown in Figure 5-9. From the literature review it is known, that NO_x is expected to be high when CO is low and vice versa. The two points in the circles do not follow this expected trend. These two data points are the same points circled in Figure 5-8. In Appendix B, Figure B-5 shows a plot similar to Figure 5-8 without the two "outliers". The R^2 value without these two points became 0.97. Consequently, these two data points were removed from the data set.

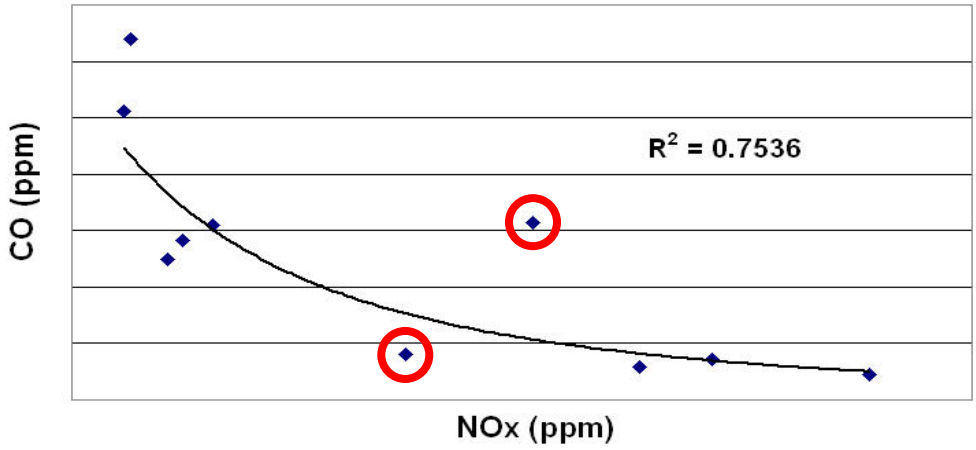

Figure 5-9 NO_x versus CO

Figure 5-10 shows gas producer speed versus CO emissions. Although the R^2 value of the power trend line is close to one, two data points at half load show a significantly higher amount of CO with a difference of 20 and 30 ppm. The CO emissions data points at full load are all within a range of 3 ppm.

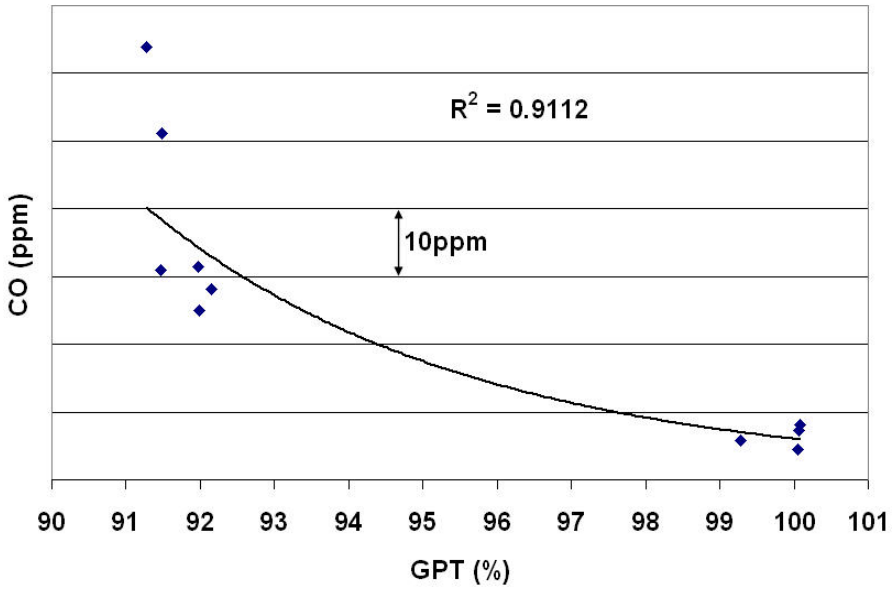

Figure 5-10 Gas producer turbine speed versus CO

The explanation for the variance of CO at low load can be seen in Figure 5-11, which shows the T_5 average versus CO. At the two high CO emissions points, the T_5 average was lower than for the other CO data points at a similar speed. A lower T_5 indicates to a lower combustion temperature.

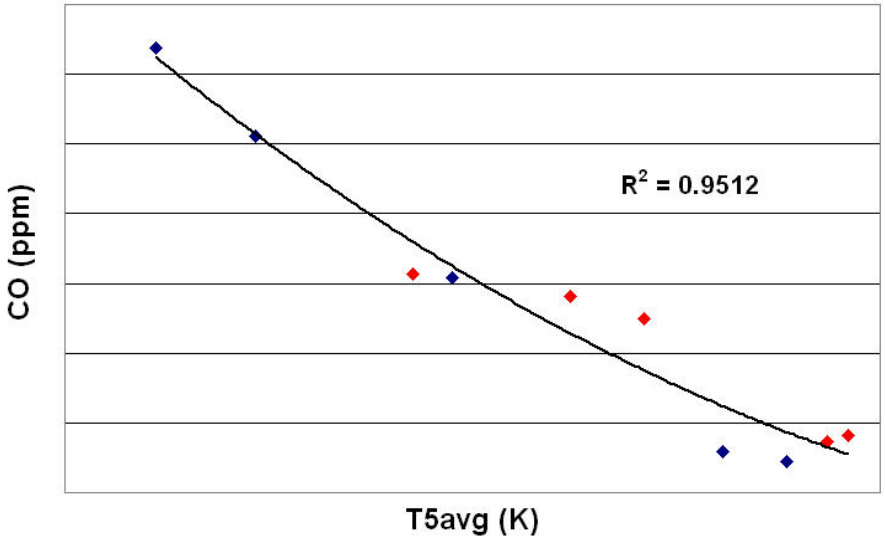

Figure 5-11 T5avg versus CO

Summery Validation

The SoLoNOx combustion system keeps the combustion temperatures within 20 Kelvin constant between half and full load. At full load, the bleed valve is completely closed and the pilot flame is low. At half load, around 13 percent of the air leaves the combustion chamber through a bleed valve and the pilot burner is used to control the temperature. Increasing the pilot fuel increases the combustion temperature vice versa. Low combustion temperatures cause higher CO emissions. CO emissions typically are the highest a low load and the lowest at full load while NOx is approximately 10 ppm higher at full load. The SOLAR test cell data is used as comparison for the developed model. The results of the comparison are in the next Chapter.

CHAPTER 6 - Results

This chapter shows the comparison of the validated test data with the results of the developed model. The chapter is divided into a performance and emission section.

Performance

The developed FORTRAN code first was compared to the temperatures and pressures given by the test data. Figure 6-1 shows a graph of gas producer speed versus temperature T_2, the combustor inlet temperature. The predicted temperature by the FORTRAN code matches the test data temperature points within 3 Kelvin.

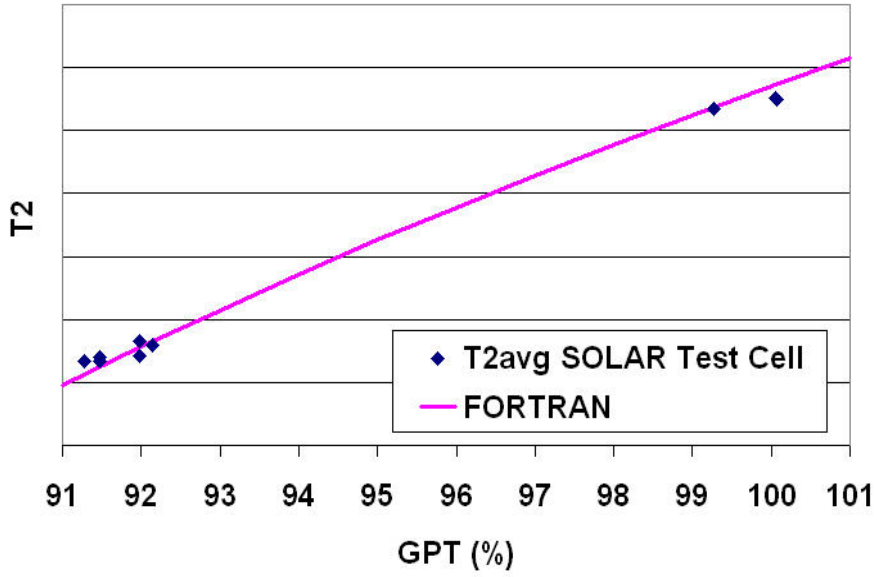

Figure 6-1 GPT versus T2

A similar graph to Figure 6-1 is shown in Figure B-7 in Appendix B. This graph shows the comparison between the measured and the predicted compressor ratio with also a high accuracy.

Fuel flow and air flow are given by the data spread sheet and can be predicted with the linear functions for any load. But how much air goes into the combustor zone and how much air is used for cooling is unknown. Known is that the adiabatic flame temperature should be around 1,800 Kelvin. Using methane as fuel, this temperature is achieved with an equivalence ratio $\phi \approx 0.65$. The air split inside the combustor has a large influence on the combustor output temperature

Also known from the data spread sheet is the temperature between the gas producer turbine and the power turbine, T_5. T_5 is the average of 12 temperature samples. The temperature differences between the samples can be up to 40 Kelvin. T_5 shown from the test is the average temperature. A 5 Kelvin difference in the model prediction seems to be not very significant.

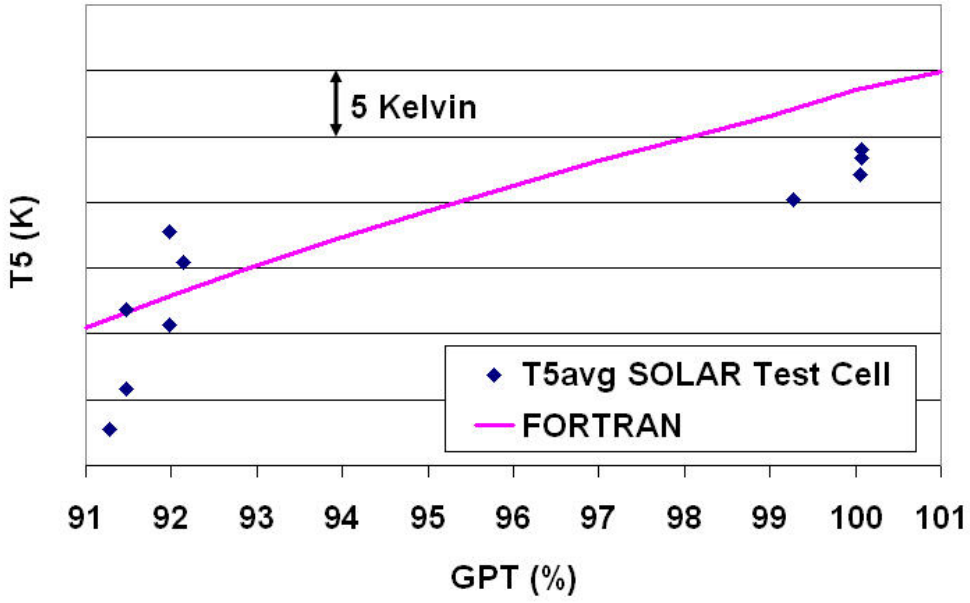

Figure 6-2 GPT versus T5

Emissions

The first correlation used by Kombust to predict the NO_x emission was derived by Lewis, Equation(2.54) from chapter 2. A constant c_{Lewis} , a function of load, was applied to the original proposed equation.

$$NO_x = 3.32 \times 10^{-6} \exp(0.008 T\, c_{Lewis}) P^{0.5} \tag{6.1}$$

A second NO_x correlation proposed by Rokke, Equation(2.56) in Chapter 2, is used as a second NO_x prediction. From the original form of the equation, only the constant value had to be reduced. The c_{Rokke} has a constant value at any load.

$$NO_x = c_{Rokke}\, P^{1.42} \dot{m}_a^{\,0.3} FA^{0.72} \tag{6.2}$$

Figure 6-3 shows with blue squares the eight NO_x data points of the test cell data. With small changes in the original proposed Equations by Rokke and Lewis, excellent correlation between the test data and the computer model was achieved.

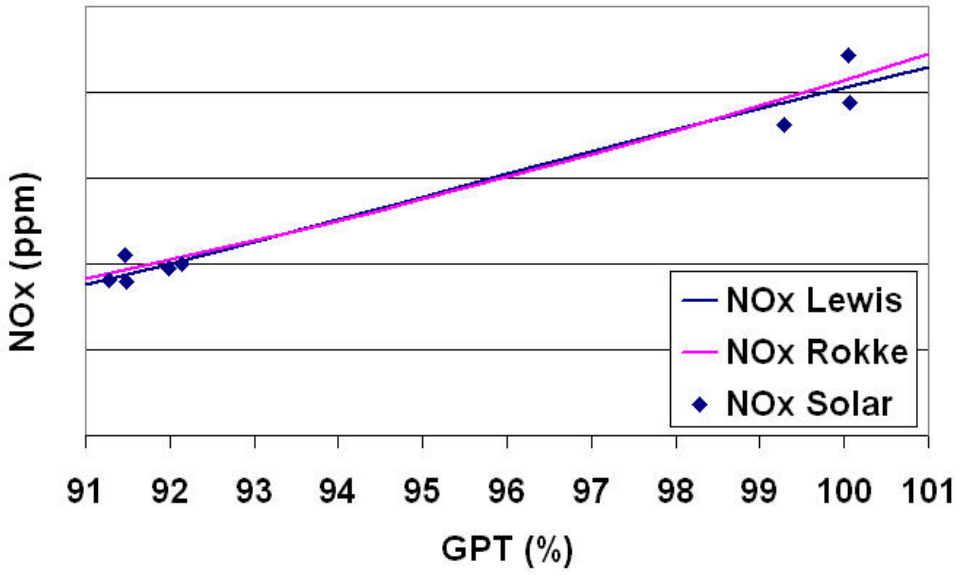

Figure 6-3 GPT versus NOx

The Kombust code has two CO correlations included, one is proposed by Rizk, one developed by Lefebvre. The correlations were developed for aircraft engines and depend on the evaporation time of the fuel. For natural gas fired gas turbines, this term is replaced in both equations by a constant. Both constants depend on the load.

Rizk correlation is modeled as:

$$\mathrm{CO} = \frac{0.18\times 10^{9}\, e^{(\frac{7800}{T_{pz}})}}{P^{2}(c_{Rizk})(\frac{\Delta P}{P})^{0.5}} \tag{6.3}$$

The CO correlation proposed by Lefebvre is used as:

$$\mathrm{CO} = \frac{86\,\dot{m}_{a}\,T_{pz}\,e^{-(0.00345T_{pz})}}{(V_{c}-c_{Lefebvre})(\frac{\Delta P}{P})^{0.5}P^{1.5}} \tag{6.4}$$

With the two correlations, excellent predictions were achieved at high load, shown in Figure 6-4. Both correlations follow the same trend. The CO predicted by Lefebvre seems to increase faster at lower load.

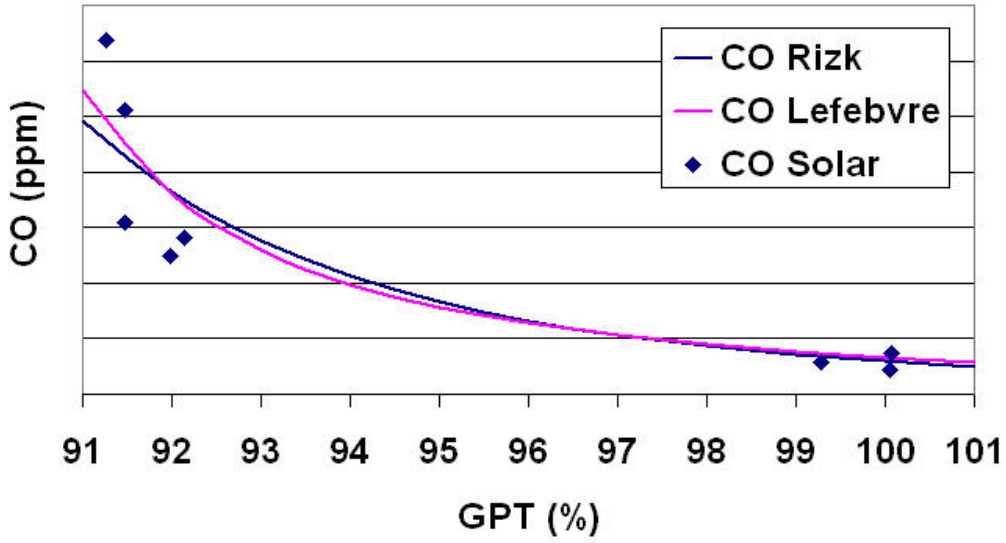

Figure 6-4 GPT versus CO

The higher amount of CO is because of a lower combustion temperature. Figure 6-5 shows that the same effect can be simulated with the FORTRAN model by adjusting the pilot burner of the model to achieve the same CO levels of the test data. The numbers in percentage shows how much fuel of the total fuel is used for the pilot burner. More pilot fuel increases the combustion temperature. This will lower the amount of CO emissions.

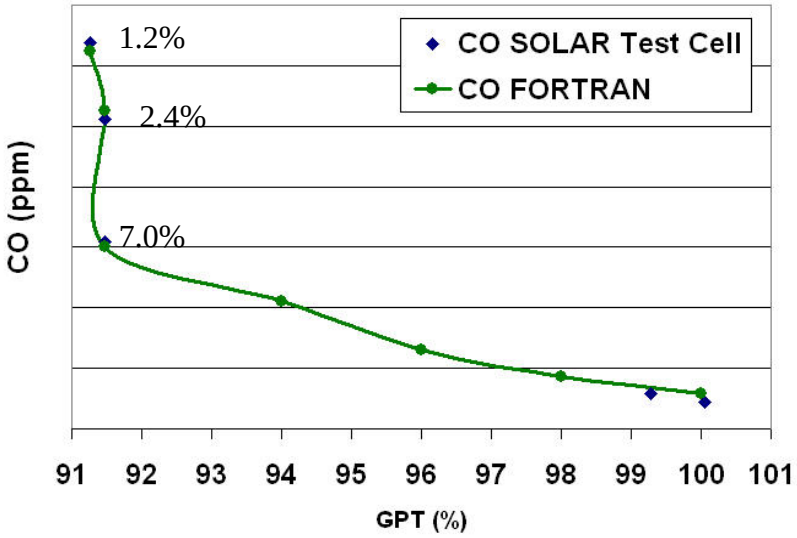

Figure 6-5 GPT versus CO with corrected pilot

Figure 6-6 shows the predicted NO_x emissions of two different ambient temperatures, at 290 Kelvin and 280 Kelvin. A lower ambient temperature decreases the combustion temperature which lowers the NO_x emissions (Lefebvre. 1999).

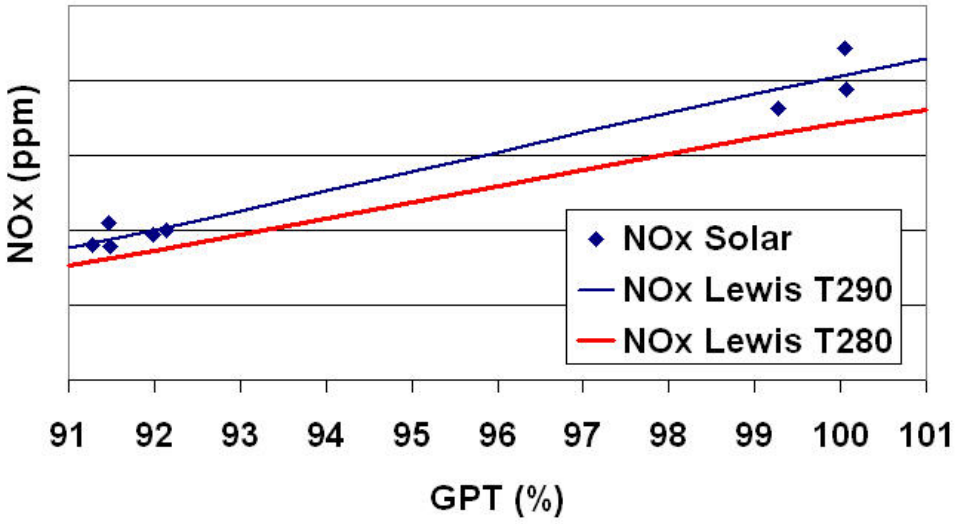

Figure 6-6 GPT versus NO_x at ambient temperature 280 and 290 Kelvin

Summary Results

The correlations used for NO_x and CO were, based on the developed mathematical model, able to predict the emissions within 2 – 3 ppm at full load. At half load, the predicted NO_x was within a range of 2 ppm to the data set. To predict CO at half load, the pilot fuel must be increased or lowered for better correlation.

CHAPTER 7 - Conclusion

A computer model based on first engineering principles was developed to predict the emissions of a dry low NO_x gas turbine combustor. The following conclusions were derived:

- Compared to a SOLAR Taurus 70 gas turbine test cell data set, good correlations between predicted and measured NO_x emissions were achieved. Both of the two different used NO_x correlations predicted the amount of NO_x at full and half load between 2 - 3 ppm to the test data emissions.
- A good prediction also was made for CO emissions at full load. The difference between test data and predicted CO emissions is within 2 ppm. Because of the high variance of CO at half load, only an average of CO could be found. The variance of CO in the data is due to the adjustment of the pilot burner at half load.
- More pilot fuel increases the combustion temperature and lowers the CO emissions versus a lower pilot fuel stream that increases the CO. The same effect was predicted by the model, where with the change of the pilot fuel, good correlations of CO were received.
- The model followed the expected trend were lowering the ambient temperature also lowered the NO_x.

The next step in this research should now be a more comprehensive comparison of the model to other sets of data. At the moment, only data points at full and half load have been available. This is not enough for a fine tuned model which would be ready for field testing. Finer tuning has to be done. The effect of changing ambient conditions could be further investigated. The existing cold ambient temperature file could be a useful data set there.

CHAPTER 8 - References

Bakken, L. E., and Skogly, L., 1995, "Parametric Modelling of Exhaust Gas Emission from Natural Gas Fired Gas Turbines," Proceedings of the International Gas Turbine and Aeroengine Congress and Exposition, Anonymous ASME, New York, NY, USA, Houston, TX, USA, pp. 11.

Becker, T., and Perkavec, M. A., 1994, "The Capability of Different Semianalytical Equations for Estimation of NO_x Emissions of Gas Turbines," Proceedings of the International Gas Turbine and Aeroengine Congress and Exposition, Anonymous Publ by ASME, New York, NY, USA, Hague, Neth, pp. 1-12.

Boyce, M.P., 2002, "Centrifugal Compressors : a Basic Guide," PennWell, Tulsa, OK, pp. ISBN: 0-87814-801-9.

Çengel, Y.A. Boles, M.A., 2002, "Thermodynamics : an Engineering Approach," McGraw-Hill, Boston, pp. ISBN: 0-07-238332-1.

Corr, R. A., Malte, P. C., and Marinov, N. M., 1991, "Evaluation of NO_x Mechanisms for Lean, Premixed Combustion," International Gas Turbine and Aeroengine Congress and Exposition, Anonymous Publ by ASME, New York, NY, USA, Orlando, FL, USA, pp. 12.

Correa, S.M., Sanjay, M., 1991, "Lean Premixed Combustion for Gas-Turbines: Review and Required Research," Proceedings of the 14th Annual Energy-Sources Technology Conference and Exhibition, Anonymous Publ by ASME, New York, NY, USA, Houston, TX, USA, 33, pp. 1-9.

Fenimore, C. P., Hilt, M. B., and Johnson, R. H., 1971, "Formation and Measurements of Nitrogen Oxides in Gas Turbines," 12(4) pp. 38-41.

Ferguson, C. R. Kirkpatrick, A. T., 2001, 2nd, "Internal Combustion Engines : Applied Thermosciences," John Wiley & Sons, New York, pp. ISBN: 0-471-35617-4.

Heywood, J.B., 1988, "Internal Combustion Engine Fundamentals," McGraw-Hill, New York, pp. ISBN: 0-07-028637-x.

Hung, W. S. Y., and Langenbacher, F., 1995, "PEMS: Monitoring NO_x Emissions from Gas Turbines," Proceedings of the International Gas Turbine and Aeroengine Congress and Exposition, Anonymous ASME, New York, NY, USA, Houston, TX, USA, pp. 9.

Hung, W. S. Y., 1991, "Predictive NO_x Monitoring System for Gas Turbines," International Gas Turbine and Aeroengine Congress and Exposition, Anonymous Publ by ASME, New York, NY, USA, Orlando, FL, USA, pp. 7.

Hung, W. S. Y., 1975a, "An Experimentally Verified NO_x Emission Model for Gas Turbine Combustors," American Society of Mechanical Engineers (Paper), (75) pp. 11.

Hung, W. S. Y., 1975b, "Reduction of NO_x Emissions from Industrial Gas Turbines," Combustion and Flame, pp. 161-181.

Jones, A, and Witherspoon, L., 2005, “Emissions Compliance Monitoring Options for Mid-Range Industrial Combustion Turbines”, Gas Machinery Conference 2005.

Ott, R. L., Longnecker, M. T., 2004,“A First Course in Statistical Methods”, Thomson Brooks/Cole, ISBN: 0-534-40806-0.

Kurz, R., and Ohanian, S., 2003, "Modeling Turbomachinery in Pipeline Simulations," PSIG 35th Annual Meeting.

Lefebvre, A. H., 1984, "Fuel Effects on Gas Turbine Combustion - Liner Temperature, Pattern Factor and Pollutant Emissions." AIAA/SAE/ASME 20th Joint Propulsion Conference. Journal of Aircraft, ed. AIAA, New York, NY, USA, Cincinnati, OH, Engl, pp. 18.

Lefebvre, A.H., 1999, "Gas Turbine Combustion," Taylor & Francis, Philadelphia, ISBN: 1-56032-673-5.

Leonard, G., and Correa, S., 1990, "NO_x Formation in Premixed High-Pressure Lean Methane Flames," Fossil Fuel Combustion Symposium 1990 - Presented at the Thirteenth Annual Energy-Sources Technology Conference and Exhibition, Anonymous Publ by ASME, New York, NY, USA, New Orleans, LA, USA, 30, pp. 69-74.

Lewis, G. D., 1991, "New Understanding of NO_x Formation," Tenth International Symposium on Air Breathing Engines, Anonymous Publ by AIAA, Washington, DC, USA, Nottingham, Engl, pp. 625-629.

Lewis, G. D., 1981, "Prediction of NO_x Emissions," American Society of Mechanical Engineers (Paper), (81) pp. 5.

Marshall, A. M., Snyder, R. B., and Bautista, P., 1997, "Continuous Parametric Monitoring Systems for Gas Turbines," Proceedings of the 1997 Air & Waste Management Association's 90th Annual Meeting & Exhibition, Anonymous Air & Waste Management Assoc, Pittsburgh, PA, USA, Toronto, Can, pp. 8.

Miller, J. A., and Bowman, C. T., 1989, "Mechanism and Modeling of Nitrogen Chemistry in Combustion," Progress in Energy and Combustion Science, 15(4) pp. 287-338.

Nicol, D. G., Steele, R. C., Marinov, N. M., 1995, "Importance of the Nitrous Oxide Pathway to NO_x in Lean-Premixed Combustion," Journal of Engineering for Gas Turbines and Power, Transactions of the ASME, 117(1) pp. 100-111.

Rizk, N. K., and Mongia, H. C., 1993, "Semianalytical Correlations for NO_x, CO, and UHC Emissions," Journal of Engineering for Gas Turbines and Power, Transactions of the ASME, 115(3) pp. 612-619.

Rokke, N. A., Hustard, J. E., and Berg, S., 1993, "Pollutant Emissions from Gas Fired Turbine Engines in Offshore Practice-Measurements and Scaling," International Gas Turbine and Aeroengine Congress and Exposition, Anonymous Publ by ASME, New York, NY, USA, Cincinnati, OH, USA, pp. 10.

Sonntag, R.E., Borgnakke, C., and Van Wylen, G.J., 1998, "Fundamentals of Thermodynamics," Wiley, New York.

Stoecker, W.F., 1989, "Design of Thermal Systems," McGraw-Hill, New York, pp. ISBN: 0-07-061620-5.

Toof, J. L., 1985, "Model for the Prediction of Thermal, Prompt, and Fuel NO_x Emissions from Combustion Turbines," 30th International Gas Turbine Conference and Exhibit. Anonymous ASME, New York, NY, USA, Houston, TX, USA, pp. 8.

Turns, S.R., 2000, "An Introduction to Combustion: Concepts and Applications," WCB/McGraw-Hill, Boston, pp. ISBN: 0-07-235044-x.

APPENDICES

Appendix A - SOLAR Taurus 70

Solar Turbines
A Caterpillar Company

TAURUS 70
Gas Turbine Mechanical-Drive Package

OIL & GAS

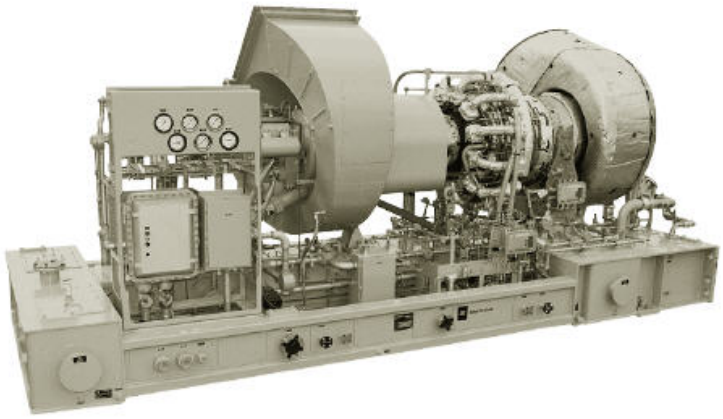

General Specifications

***Taurus*™ 70 Gas Turbine**

- Industrial, Two Shaft
- Axial Compressor
  - 14 Stage
  - Variable Inlet Guide Vanes
  - Compression Ratio: 16:1
  - Inlet Airflow: 26.5 kg/sec (58.5 lb/sec)
  - Axially Split Case
- Combustion Chamber
  - Annular Type
  - Conventional or Lean-Premixed, Dry, Low Emission (*SoLoNOx*™)
  - 12 Fuel Injectors
  - Torch Ignitor System
- Gas Producer Turbine
  - 2 Stage, Reaction
  - Speed: 15,200 rpm
- Power Turbine
  - 2 Stage, Reaction
  - Speed: 12,000 rpm
- Bearings
  - Journal and Thrust: Tilting Pad
- Coatings
  - Compressor Stators and Drums: Inorganic Aluminum
  - Turbine Nozzles and Blades: Precious Metal Diffusion Aluminide
- Axial Position Probes, Proximity Probes, Keyphasors and RTDs

Key Package Features

- Driver Skid with Drip Pans
- 316L Stainless Steel Piping ≤102mm (4")
- Compression-Type Tube Fittings
- Digital Display Panel
- Electrical System Options
  - NEC Class I, Group D, Div. 1 or 2
  - CENELEC Zone 1 or 2
- *Turbotronic*® Microprocessor Control System
  - Offskid or Onskid ControlNet 1.5
  - Video Display Unit
  - Temperature and Vibration Monitoring
  - Historical Displays
- Control System Options
  - Auxiliary Control Interface or Auxiliary Control Console (with onskid controls)
  - Remote Control and Display
  - 120-VDC Control Battery/Charger
  - Supervisory Communications Interface
  - Turbine Performance Map
  - Printer/Logger
  - Field Programming
  - Process Controls
  - Compressor Performance Map
  - Compressor Anti-Surge Control
- CE/ATEX Zone 2 Certification
- Start Systems
  - Pneumatic
  - Direct Drive AC
- Fuel System: Natural Gas
- Integrated Lube Oil System
  - Turbine-Driven Accessories
  - Oil Tank Vent Separator
  - Oil Tank Vent Flame Trap
- Lube Oil System Options
  - Oil Cooler
  - Oil Heater
- Compressor Cleaning System Options
  - On-Crank
  - On-Crank/On-Line
  - Certified Cleaning Tank
- Gearbox (if applicable)
  - Speed Increaser or Reducer
- Air Inlet and Exhaust System Options
- Enclosure and Associated Options
- Factory Testing of Turbine and Package
- Documentation
  - Mechanical and Electrical Drawings
  - Quality Control Data Book
  - Inspection and Test Plan
  - Test Reports
  - Operation and Maintenance Instruction Manual

Solar Turbines
A Caterpillar Company

TAURUS 70

Gas Turbine Mechanical-Drive Package

OIL & GAS

Performance

Output Power	7690 kW (10,310 hp)
Heat Rate	10 340 kJ/kW-hr (7310 Btu/hp-hr)
Exhaust Flow	95 630 kg/hr (210,830 lb/hr)
Exhaust Temp.	495°C (920°F)

Nominal Rating – ISO
At 15°C (59°F), sea level

No inlet/exhaust losses

Relative humidity 60%

Natural gas fuel with
LHV = 31.5 to 43.3 MJ/nm³
(800 to 1100 Btu/scf)

Optimum power turbine speed

AC-driven accessories

Engine efficiency: 35.7%

15°C (59°F) turbine rating match
Other turbine rating match points available

Available Power

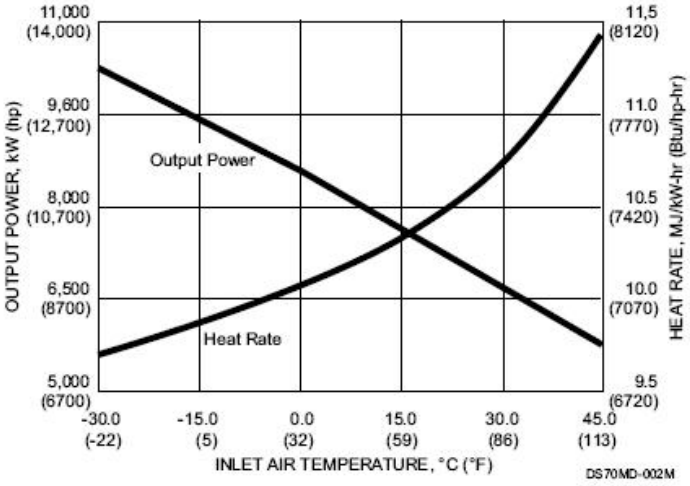

Package Dimensions

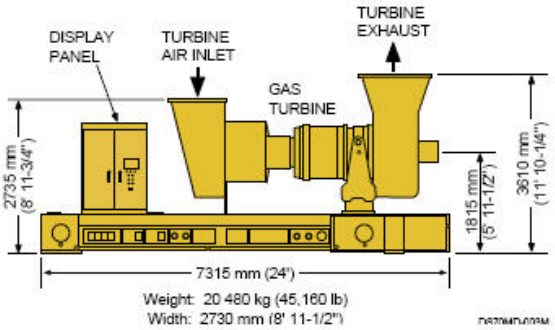

Solar Turbines Incorporated
P.O. Box 85376
San Diego, CA 92186-5376

DS70MD/505/EO

FOR MORE INFORMATION

Telephone: (+1) 619-544-5352
Telefax: (+1) 619-544-2633
Internet: www.solarturbines.com

DNV

Appendix B - Test Cell Graphs for Mass Flow and Emissions

Mass Flow

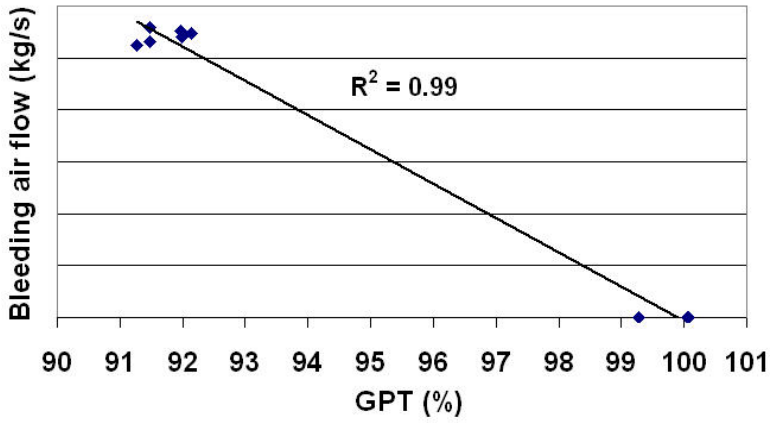

Figure B-1 Gas producer turbine speed versus bleeding air flow

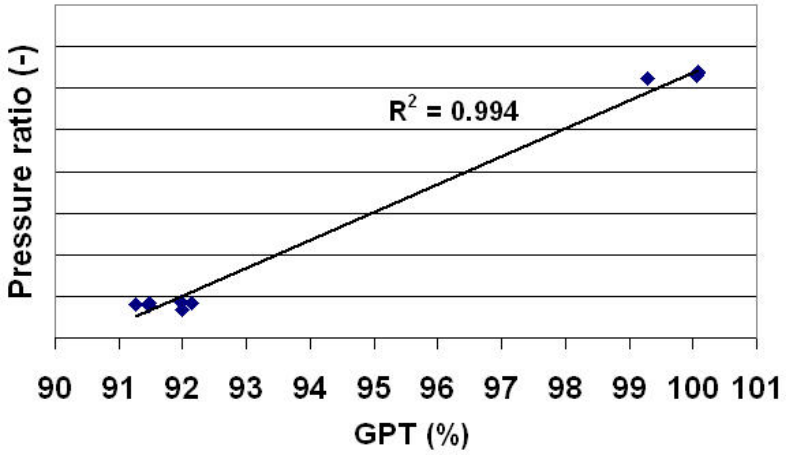

Figure B-2 Gas producer turbine speed versus pressure ratio compressor

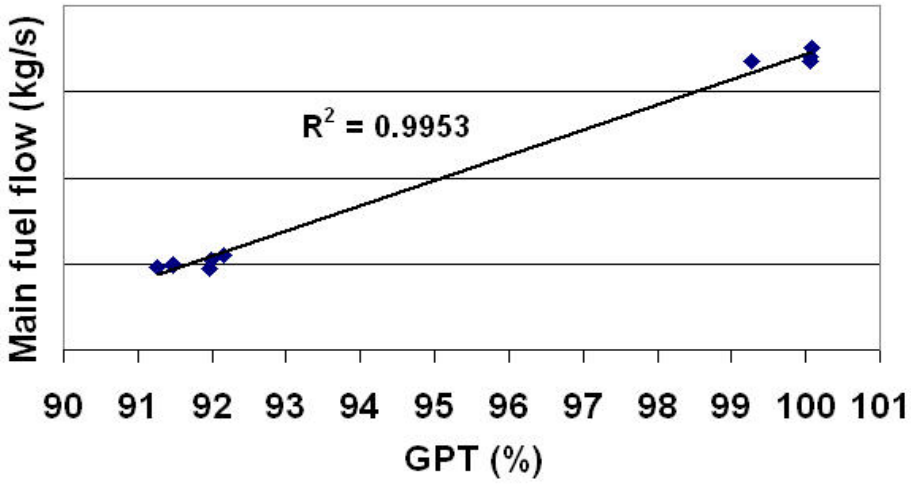

Figure B-3 Gas producer turbine speed versus main fuel flow

Emission

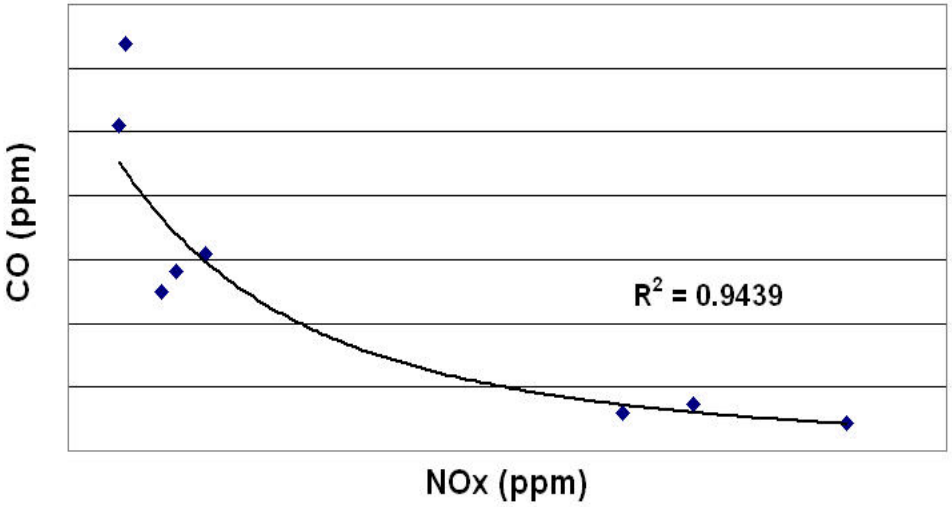

Figure B-4 NO_x versus CO without the two "outliners"

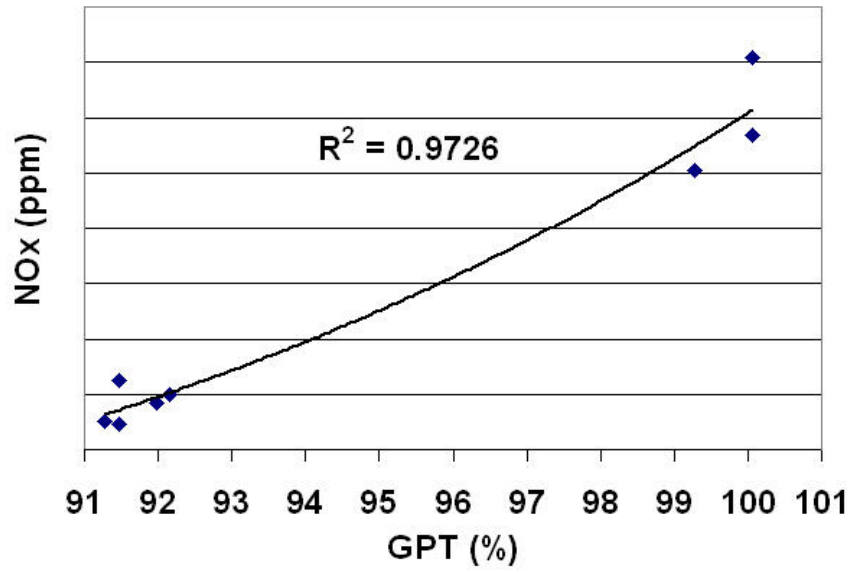

Figure B-5 GPT versus NO_x without the two "outliners"

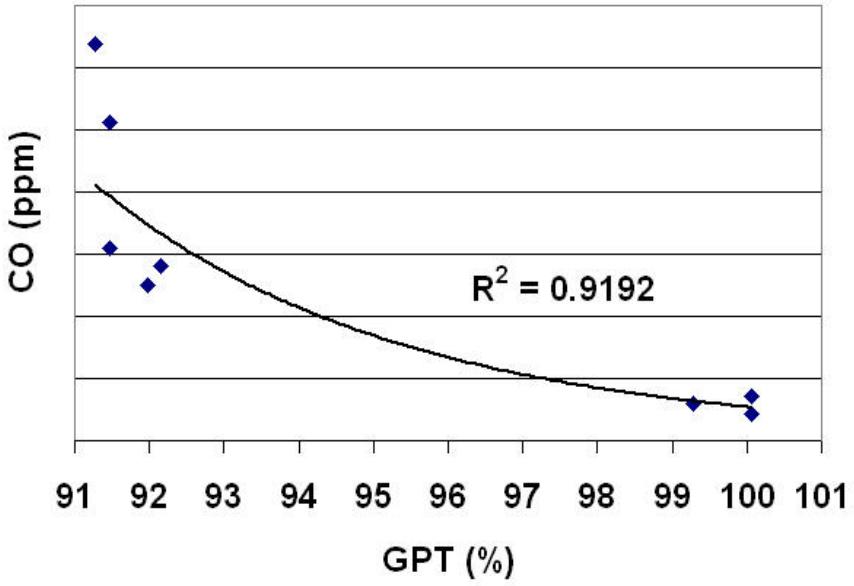

Figure B-6 GPT versus CO without the two "outliners"

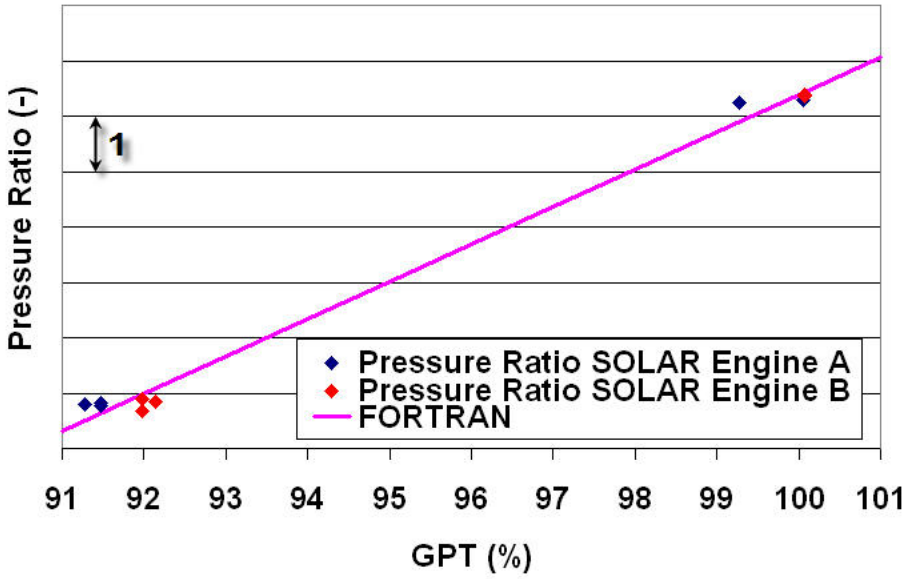

Figure B-7 GPT versus pressure ratio